Amniotic ectoderm expansion occurs via distinct modes and requires SMAD5-mediated signalling

Mariya P. Dobreva[1,2,7,8,*], Vanesa Abon Escalona[1,2,3,7], Kirstie A. Lawson[4*], Marina N. Sanchez[2], Ljuba C. Ponomarev[3], Paulo N.G. Pereira[1,2], Agata Stryjewska[5], Nathan Criem[1,2,3], Danny Huylebroeck[5], Susana M. Chuva de Sousa Lopes[6], Stein Aerts[2], An Zwijsen[1,2,3,*]

[1] VIB Center for the Biology of Disease, Leuven, 3000, Belgium

[2] Department Human Genetics, KU Leuven, Leuven, 3000, Belgium

[3] Department of Cardiovascular Sciences, KU Leuven, Leuven, 3000, Belgium

[4] MRC Human Genetics Unit, the MRC Institute of Genetics and Molecular Medicine, University of Edinburgh, Edinburgh, EH4 2XU, UK

[5] Department of Development and Regeneration, KU Leuven, Leuven, 3000, Belgium

[6] Department of Anatomy and Embryology, Leiden University Medical Center, Leiden, 2333 ZC, the Netherlands

[7] Contributed equally to this work

[8] Present address: Department of Life Sciences, Imperial College London, Silwood Park Campus, Ascot, Berkshire SL5 7PY, United Kingdom

Lead contact: An Zwijsen

* Correspondence: m.dobreva@imperial.ac.uk, kirstie.lawson@igmm.ed.ac.uk, and an.zwijsen@kuleuven.be

ABSTRACT

Upon gastrulation, the mammalian conceptus transforms rapidly from a simple bilayer into a multi-layered embryo enveloped by its extraembryonic membranes. Impaired development of the amnion, the innermost membrane, causes major malformations. To clarify the origin of the mouse amnion, we used single cell-labelling and clonal analysis. We identified four clone types with distinct clonal growth patterns in amniotic ectoderm (AmEc). Two main types have progenitors in extreme proximal-anterior epiblast. Early descendants initiate and expand AmEc posteriorly, while descendants of cells remaining anteriorly later expand AmEc from its anterior side. Amniogenesis is abnormal in embryos deficient in the BMP signalling effector SMAD5, with delayed closure of the proamniotic canal, and aberrant amnion and folding morphogenesis. Transcriptomics of individual *Smad5* mutant amnions isolated before visible malformations, and tetraploid chimera analysis, revealed two amnion defect sets. We attribute them to impairment of progenitors of the two main cell populations in AmEc and to compromised cuboidal-to-squamous transition of anterior AmEc. In both cases, SMAD5 is critical for expanding AmEc rapidly into a stretchable squamous sheet to accommodate exocoelom expansion, axial growth and folding morphogenesis.

Summary statement: Clonal analysis shows that four distinct progenitor groups expand normal amnion differently. In SMAD5 deficient mice, undersized and abnormally non-squamous amnion involves at least two impaired progenitor groups.

INTRODUCTION

Animals classified as amniotes, including reptiles, birds and mammals, develop extraembryonic tissues and organs that perform respiration-related, nutritional and protective functions during embryogenesis: these are chorion, yolk sac, amnion and allantois. Alongside their supportive role, extraembryonic tissues take part in the development of the early embryo proper by providing signalling cues and spatial continuity (Horn and Panfilio, 2016; Mesnard and Constam, 2010; Shao et al., 2016). The amnion is the innermost extraembryonic tissue that delineates the fluid-filled amniotic cavity providing space for the embryo to move freely. The amnion protects the embryo against traumas, infections and toxins (Schmidt, 1992). Despite its location at the extraembryonic-embryonic interface, the amnion has classically not been considered a driving force in shaping the early embryo proper. However, in mice, the expansion of the amniotic cavity is critical for the reorientation of notochord cells along the anterior-posterior axis and for the global morphogenesis of the early embryo (Imuta et al., 2014). Furthermore, in chickens the physical expansion of (pro)amnion is required for the correct positioning of the head (de Melo Bernardo and Chuva de Sousa Lopes 2014). In humans, impaired amnion integrity, premature rupture of amnion and amniotic bands often cause preterm birth and fetal malformations including amputations and fetal compression syndromes (Menon and Richardson, 2017; Opitz et al., 2015). Despite the importance of amnion, its developmental origin and the molecular regulation of amniogenesis remain ill-defined.

In the mouse, amnion and chorion development are intimately related. Early during gastrulation, at embryonic day (E)6.5-7.0, extraembryonic mesoderm emerging from the most posterior part of the primitive streak (further called "streak") accumulates in the incipient fold at the posterior extraembryonic-embryonic junction. This amniochorionic fold gives rise to both amnion and chorion, but initially consists only of (prechorionic) extraembryonic ectoderm. The epiblast-derived amniotic ectoderm contributes relatively late, and only to the floor of the fold. The cuboidal chorionic ectoderm thus greatly exceeds the squamous amniotic ectoderm portion of the fold at all stages (Pereira et al., 2011). The extraembryonic mesodermal layer, still shared by the future amnion and chorion, develops from the accumulating posterior mesoderm and lines the expanding exocoelomic cavity. When the fold is fully expanded, the chorionic walls of the proamniotic canal fuse at the extraembryonic-embryonic junction at the embryo's anterior side, the anterior separation point (Pereira et al., 2011). This causes amnion-chorion separation, and partition of the proamniotic cavity into the amniotic, exocoelomic and ectoplacental cavities at E7.5. Shortly after amnion-chorion separation, foregut invagination begins, marking the onset of ventral folding morphogenesis. The flexible amniotic membrane envelops the entire embryo only on completion of ventrolateral morphogenesis and body wall closure (Schmidt, 1992).

Several studies indicate that bone morphogenetic protein (BMP) signalling at the extraembryonic-embryonic interface is important for amnion-chorion separation and amnion development in the mouse (reviewed in (Pereira et al., 2011)). Binding of BMPs to their receptors triggers activation by phosphorylation of SMAD1, -5 and -9 that co-regulate BMP-responsive gene expression (Katagiri and Watabe 2016). SMAD5 deficient embryos develop severe morphogenesis defects (Chang et al., 1999; Yang et al., 1999), amnion-chorion separation is delayed and the anterior separation point is shifted posteriorly (Bosman et al., 2006). After closure of the proamniotic canal, a striking aggregate of cells develops anteriorly in the amnion (Chang et al., 1999). These aggregates ectopically express the mesoderm inducer *Nodal*, in addition to *T, Fgf8* and *Eomes,* all established streak mesoderm markers (Pereira et al., 2012). The aggregates are variable in size, position and relative composition at E8.5-E9.0. In contrast to the avascular wild-type amnion, the aggregates become vascularized and develop red blood cells and primordial germ cell (PGC)-like cells (Bosman et al., 2006; Chang et al., 1999), all posterior streak derivatives. BMP-SMAD signalling is active during amniogenesis as shown in a *BRE::LacZ* reporter mouse that monitors transcriptional activity of phosphorylated BMP-SMADs (Cajal et al., 2014; Dobreva et al., 2012). Reporter activity is present in the amniotic ectoderm component of the amniochorionic fold, the separated amnion, the anterior midline region distal from the extraembryonic-embryonic junction and, from amnion-chorion separation onwards, in the lateral junctions of amnion with surface ectoderm. BMP-SMAD signalling is also critical in other species for amnion-like tissue development, e.g. in amniogenesis in human pluripotent stem cell cultures (Shao et al., 2016), and in defining amnion and serosa or amnioserosa in different insect species (Rafiqi et al. 2012; Horn and Panfilio 2016). Furthermore, prominent amniotic expression of *BMP4* has been reported in cynomolgus monkeys (Sasaki et al., 2016).

Little is known about the developmental origin of the amnion, particularly the amniotic ectoderm (Kinder et al., 2001; Lawson et al., 1991). To remedy this, we made a prospective lineage analysis by labelling single epiblast cells (Lawson et al. 1991) in the proximal half of wild-type mouse embryos before and early in gastrulation (E6.2-E6.5). We identified four distinct types of clonal growth pattern that expand amniotic ectoderm differently and with different magnitude. Additionally, we investigated the earliest steps of abnormal amniogenesis in mice deficient in SMAD5 by sequencing the mRNA (RNA-seq) of individual control and mutant amnion samples, and by chimera analysis. Correlating these data with the clonal analysis supports the conclusion that the impaired amniogenesis in *Smad5* mutants results from the two main cell populations in amniotic ectoderm being affected by the SMAD5 deficiency.

RESULTS

Amniotic ectoderm is derived from the proximal-anterior and anterolateral epiblast

To gain insight into the location of amnion progenitors and to trace their contribution in amniotic ectoderm, we labelled single epiblast cells in the proximal half of wild-type embryos at PS (prestreak) and ES (early streak) stages and analysed the resulting clones. Two properties of single-cell labelling followed by short-term retrospective lineage analysis were exploited in this approach. Firstly, labelling by iontophoretic injection enables analysis of clones with known spatial and temporal origins. It gives fine resolution fate maps and the opportunity to reconstruct morphogenetic change from patterns of clonal expansion during a period of rapid growth. Secondly, lineage analysis of prospectively labelled clones allows the clonal history to be inferred within the cell layer of origin. Thus, the time trajectory within the amniotic ectoderm, which is continuous with the epiblast within which the clone arose, can be traced with confidence retrospectively.

The fate maps of PS and ES stages show that the amniotic ectoderm is derived mainly from mixed fate progenitors in the proximal anterior and anterolateral epiblast, while amniotic mesoderm progenitors, also of mixed fate, lie more posteriorly and distally. These findings are graphically displayed in **Fig. 1**. From the triangular-shaped region spanning the anterior midline that generated amniotic ectoderm, only a minority of labelled descendants (8%, 245/3032 from 61 clones) were in amniotic ectoderm. Not all epiblast cells in this region gave rise to amniotic ectoderm, but the composition of clones was otherwise indistinguishable from that of their amnion-contributing neighbours. This showed an anterior-posterior transition in the fate map from predominantly surface ectoderm to extraembryonic mesoderm (**Fig. 1**, comparing upper and lower panels). The amniotic ectoderm therefore develops from a relatively small number of descendants of proximal-anterior and anterolateral epiblast that, before and at the onset of gastrulation, is mainly prospective surface ectoderm and extraembryonic mesoderm.

Amniotic ectoderm is established via several routes

The detailed findings from the 28 clones that contributed to amniotic ectoderm are presented in **Fig. 2, Table 1** and **Fig. S1**. Overall, four clone types were distinguished on the basis of their distribution within the amniotic ectoderm (**Fig. 2**) and clone composition (**Table 1**).

Type I clones originated in a very restricted region of extreme proximal anterior/anterolateral epiblast, abutting the extraembryonic ectoderm: they were mixed clones with descendants mainly in extraembryonic structures, posterior streak and PGCs (**Table 1**). Type I clones were rare and only found at PS stage, see **Fig. S2** for possible explanations. These clones spread in the amniotic ectoderm from

the ASP to the posterior edge of the amnion indicating that they contributed to the amnion from its inception: the position of the most anterior cells of these clones reflected the origin of the progenitors in association with presumptive chorionic ectoderm. The first amniotic cell of the clone would have been an extreme posterior (proximal) epiblast or posterior streak cell in contact with the floor of the early amniochorionic fold; it then divided, leaving one daughter associated with the prechorionic ectoderm, the other with the epiblast/streak. Succeeding divisions then expanded the amniotic portion of the fold. Clones #1 and #2 must have gone through two cell generations in the epiblast before contributing one cell (clone #1), or one followed by two (clone #2), to the emergent amnion between E6.8-7.1 (**Fig. S1A**) at midstreak (MS) to late streak (LS) stages (see Lawson and Wilson, 2016, Fig. 3.5 for correlation of age and stage). Subsequently, the clone expanded through the following three or two generations respectively (**Fig. S1A**). The distribution pattern of Type I clones indicates that these clones represent the founding population of the amniotic ectoderm until amnion closure.

Type II clones originated over a larger area of proximal-anterior epiblast than Type I. These mixed clones contributed mainly to extraembryonic mesoderm, posterior streak, and PGCs with generally only a small minority of descendants in amniotic ectoderm (**Table 1**)**.** The contribution was limited to posterior amnion (**Fig.2**), was slightly later than Type I and over a longer period (E7.2-E8.1) (**Fig. S1B**). Hence, Type II descendants moved into the established primordium and remained as short files that had not extended further than 15% of the anterior-posterior length of the amnion by early somite stages (**Fig. 2**). At the LS stage, the amnion ectoderm consists of only about 20 cells (EMA10 eMouseAtlas (Armit et al., 2017)) and, given the behaviour of Type II clones, the founding population associated with the chorionic ectoderm is probably complete by this time. Therefore, the founding population of the amniotic ectoderm appears to be both small and established within a narrow time window.

Type III clones originated in the proximal quadrant of epiblast spanning the anterior midline i.e. in prospective surface ectoderm, which was the main clonal component. Single, small inclusions of labelled cells in the periphery of the amnion were found between the axial level of the midbrain and the node (**Fig. 2**). The size of the inclusion expanded with the rest of the clone. The inferred clonal histories (**Fig. S1C**) indicate that the inclusion of 2 cells would have occurred between E7.3 and 7.7, (expected early pre-headfold (EPHF) to late headfold (LHF)) i.e. in the period of rapid amnion expansion during and after closure, onset of axial elongation from the node, expansion of the neural folds and initiation of the foregut. This suggests that inclusion into the periphery of the amnion from embryonic ectoderm is usually limited to a period when considerable adjustments to turgor in the amniotic and yolk sac cavities occur and when the rostral half of the embryo is growing rapidly.

Type IV clones originated in extreme proximal anterior to anterolateral epiblast, spanning the midline. They were generated between ES+ and MS stages within the same area as the earlier Type I clones, but were exceptional in being lineage restricted with all descendants in amniotic ectoderm (**Table 1, Fig. 2**). The pattern of clonal spread at LPHF/EHF indicated that early descendants entered the amnion at, or close to the anterior midline. They not only expanded the amniotic ectoderm anterior to the ASP, but also contributed to the main body of amniotic ectoderm laid down by the original Type I founding population (**Fig. 3A-B**). Descendants in somite stage embryos were found concentrated mainly between the axial levels of heart and hindbrain.

An interesting mixed type clone (#28) contributed to the amnion from both anterior and posterior. The inferred history (**Fig. S1D**) indicated that the ES- progenitor would have divided twice before one cell became restricted to amniotic ectoderm (behaving further as Type IV) and the remaining three cells behaved as Type II, contributing further descendants to posterior amnion, posterior streak and allantois. Together, these results indicate that extreme proximal descendants of PS or ES stage epiblast that remain anterior, become part of a relatively late population of exclusively amniotic ectoderm precursors that expand the amnion specifically from the anterior.

In brief, Type I descendants initiate amniotic ectoderm. Until closure of the proamniotic canal, Type I and II descendants, both from mixed fate progenitors, expand the amniotic ectoderm. Around the time of proamniotic canal closure and after amnion-chorion separation the amniotic ectoderm becomes extensively expanded directly from the anterior by the late contributing, lineage-restricted Type IV descendants. Type III descendants expand the amnion only at the periphery. The behaviour and timing of the different groups that constitute the amniotic ectoderm are summarized in **figures 3B** and **8A-B**.

The amnion of *Smad5* mutants expresses two transcriptionally distinct signatures

In normal early somite stage mouse conceptuses amnion appears as a translucent and stretched tissue. In contrast, most *Smad5* mutants (KOs) are distinguished by the presence of a variable aggregate of cells in the amnion. Additionally, mutants have various ventral folding defects (Chang et al., 1999) (**Fig. 4A**). Amniotic ectoderm is cuboidal before aggregate formation in contrast to the squamous control amnion, and the junction between amniotic and embryonic ectoderm is anteriorly less pronounced in all *Smad5* mutants (**Fig. 4B**).

We investigated the molecular differences between WT and *Smad5* mutant amnion by RNA-seq analysis. Amnions were microdissected (**Fig. 4C-D**) from control (n=6), and stage-matched littermate *Smad5* knockout (n=6) embryos ranging between EPHF and 3-somite (3S) stages (**Table S1**), before major morphological differences become apparent. We synthesized and amplified cDNA from individual amnion samples. Absence of contamination with surrounding tissues was confirmed by qRT-PCR marker analysis in control samples (**Fig. S3A**).

The variance-normalized counts of the RNA-seq data (**Table S1**) were used for expression visualization, clustering and differential gene expression analysis. Unsupervised clustering of all 12 samples by Principal Component Analysis (PCA) resulted in clustering of 5 out of 6 control samples and the segregation of the 6 knockout samples into two distinct groups, which we named KO-SetA and KO-SetB (**Fig. 5A**). Ctrl6.1 was determined to be an outlier and omitted from further analysis. Gene set enrichment analysis (GSEA) on the top differentially expressed genes (p.adj. <0.05) showed that KO-SetA samples were significantly enriched for categories such as "gastrulation", "mesoderm development" and "cell fate specification" whereas gene sets like "integrin binding" and "regulation of cell adhesion" were underrepresented (**Fig. S3B-C, Table S2, Supplemental Materials and Methods**). Conversely, KO-SetB samples were enriched in categories such as "placenta development" and "extraembyonic ectoderm", while "extracellular matrix" and "epithelial-to-mesenchymal transition (EMT)" sets were downregulated.

Closer examination of samples with the KO-SetA signature (**Fig. 5B-C, Table S3, Suppl. Excel file 1**) confirmed and expanded our former *in situ* hybridization results on ectopic expression of *Nodal, T, Lefty2, Wnt3* and *Fgf8* in *Smad5* mutant amnion (Pereira et al., 2012). Furthermore, KO-SetA samples significantly overexpressed several markers related to EMT, streak and streak-derived mesoderm (**Fig. 5B-C, Table S3).** They include the streak mesoderm related *Follistatin/Fst* (57-fold increase in KO-SetA compared to control), *Zic3* (79-fold); the Nodal co-receptor *Tdgf1* or *Cripto* (22-fold); and the Nodal target genes *Fgf5* (71-fold), *Mixl1* (14-fold) and *Mesp1* (18-fold). Remarkably, several extraembryonic ectoderm markers were robustly enriched in samples with KO-SetB signature (**Figs 5B-C; Table S3; Suppl. Excel file 1**). These included genes such as *Elf5* (391-fold more in KO-SetB compared to control), *Esrrb* (202-fold), *Sox 2* (15-fold), *Sox 21* (107-fold) and *Cldn3* (146-fold).

The two KO sets shared some features. Underrepresentation of genes encoding ECM components, such as collagens, and downregulation of amnion-enriched transcripts like *Postn* (Dobreva et al., 2012), *Tfap2a* and *Twist1* (Bosman et al., 2006)*,* and *Flrt3* (Egea et al., 2008), suggested loss of amnion identity (**Figs 5C; Fig. S3B-C; Table S3; Suppl. Excel file 1**). *Eomes* – a streak marker and target gene of Nodal signalling (Arnold et al., 2008) but also a marker for extraembryonic ectoderm (Ciruna and Rossant, 1999) – was found enriched in both KO-Sets. Target genes of BMP signalling like *Smoc2, Postn* (Inai et al., 2008) and *Flrt3* (Tomás et al., 2011) were underrepresented in both KO-Sets (**Table S3**), however differential expression of other target genes of BMP/SMAD5, BMP ligands and modulators of BMP signalling were specifically observed in KO-SetB samples, *e.g. Msx1*, *Hand1* and *Nog (Noggin)*.

The distribution of KO-SetA and KO-SetB expression profiles was validated by RT-qPCR in a larger cohort of 25 E7.5 littermate control-knockout amnion sample pairs. We selected 4 KO-SetA (*Fgf5, Nodal, T* and *Lefty2*) and 4 KO-SetB (*Elf5, Essrb, Cldn4* and *Sox2*) genes enriched in one but not the other set (**Table S4, Fig. 5C**). One out of 25 pairs showed only differential expression of one of the selected markers, and was therefore not categorized. The majority of the pairs (64%) segregated either into a KO-SetA (48%) or KO-SetB (16%) signature (**Fig. 5D**). Several pairs (32%) showed an intermediate signature with two or more markers (over)expressed from each set. Collectively, the data demonstrate presence of two transcriptionally distinct signatures in the amnion of *Smad5* mutants. The high prevalence of the intermediate signature suggests transition from a KO-SetB to a KO-SetA category (progressive loss of ExEc inclusion features because of ExEc transdifferentiation into an aggregate) or co-existence of mixed KO-SetA and KO-SetB phenotypes.

FGF5 and ELF5, KO-SetA and -SetB markers, are ectopically localized in mutant amniotic ectoderm
Subsequently, we documented where top-overexpressed markers of KO-SetA and -SetB localize in mutant amnion. Ectopic *T, Nodal* and *Wnt3* expression, and Nodal and β-catenin mediated signalling in amniotic ectoderm of *Smad5* mutants was previously documented (Pereira et al., 2012). Here, we show the expression of a new SetA marker, *Fgf5. Fgf5* is normally expressed in the epiblast at ES, including in the region where amniotic ectoderm precursors reside. Its expression is lost anteriorly at LSEB and *Fgf5* is absent in normal amnion (Li et al., 2013). We found *Fgf5* expressed ectopically in 9 out of 10 *Smad5* EPHF-EHF embryos. The ectopic expression was prevalent in the anterior embryonic ectoderm and continuous with the anterior amniotic ectoderm, consistent with the continuous cuboidal ectoderm shown in Fig. 4B. Its range of extension into amniotic ectoderm was variable but could reach as far posteriorly as the abnormally positioned ASP (**Fig. 6A**).

Next, we assessed the localisation of a KO-SetB marker, Elf5, an extraembryonic ectoderm-specific transcription factor (Donnison et al., 2005) and Oct4/Pou5f1, normally detected in amniotic ectoderm at EPHF stages (Downs, 2008). In E7.5 control embryos, amniotic ectoderm was Oct4-positive and Elf5-negative, while extraembryonic ectoderm showed Elf5 presence but no Oct4 (**Fig. 6B, Ctrl**). This pattern was present in the majority of the mutants (20/25) (**Fig. 6B, KO-SetA**). However, in a fraction of the mutants (5/25) a portion of ectoderm, continuous with the amniotic ectoderm, was strongly Elf5-positive and Oct4-negative (**Fig. 6B, KO-SetB**). This pattern did not correlate with a specific developmental stage (data not shown). The ectopic presence of Elf5, but also of Eomes (**Fig. S4**), in amniotic ectoderm in some mutants is suggestive of inclusion of extraembryonic ectoderm, although *de novo* transcript induction could not be excluded at this stage.

Tetraploid chimeras support aberrant expansion of amniotic ectoderm in *Smad5* mutants

Based on (i) the delayed closure of the proamniotic canal and amnion-chorion separation in *Smad5* knockout embryos (**Fig. 6**); (ii) the two different KO-Set signatures (**Fig. 5**); and (iii) the robust expression of extraembryonic ectoderm enriched transcripts in the KO-SetB samples (**Fig. 5**), we reasoned that a deficit in the amniotic ectoderm could result in compensatory inclusion of non-amniotic epiblast tissue and/or trailing extraembryonic ectoderm into the mutant amnion.

Tetraploid (4n) complementation assays were performed to determine i) whether an extraembryonic ectoderm inclusion occurs in the mutant amnion, and ii) whether such inclusions transdifferentiate into aggregates (**Fig. 7A**). Donor embryonic stem cells (ESCs) in ESC↔4n embryo chimeras normally give rise to all epiblast-derived tissues, including the extraembryonic mesoderm and amniotic ectoderm. Conversely, tetraploid descendants are restricted to trophectoderm derivatives, including chorionic extraembryonic ectoderm and extraembryonic endoderm lineages. The segregation of descendants of ESCs and tetraploid cells in a chimera thus enables a distinction to be made between cells of epiblast or extraembryonic ectoderm origin. GFP-positive (GFP+) wild-type (WT) and *Smad*5 knockout ESCs (Bosman et al., 2006) were aggregated with GFP-negative (GFP-) tetraploid embryos (**Fig. 7A**).

Amniotic ectoderm and amniotic mesoderm were indeed GFP+ in control chimeras (*WT;GFP*⁺ ESC↔4n WT)(**Figs 7B, S5A**). The majority of the knockout chimeras (**Table 2**) had uniformly GFP+ amniotic ectoderm like the other epiblast-derived tissues. In most of the E7.5 knockouts (16/21) much of the amniotic ectoderm was morphologically indistinct from the anterior embryonic ectoderm (**Figs 7C-D, S5B**). Many of these embryos (**Table 2**) displayed a "head-out" phenotype, with the anterior epiblast/future head region protruding outside the visceral yolk sac (**Figs 7C, S5B, D-E**) as if anterior

amniotic ectoderm was lacking. In a few KO chimeras (3/35, 9%) the GFP+ SMAD5-deficient posterior amniotic ectoderm appeared undersized and stretches of tetraploid (GFP-) extraembryonic ectoderm were trapped in the amnion (**Figs 7E, S5G-H**).

While nearly all conventional *Smad5* knockout embryos develop an anterior aggregate in the amnion beyond the 4-somite stage (Pereira et al., 2012), only 1/14 E8.5 knockout chimeras had an anterior aggregate (**Fig. 7D**). A more posterior thickening was observed in 5/14 knockout chimeras (**Fig. S5C, F**). Amniotic aggregates were always GFP+, confirming their embryonic origin. Therefore, Elf5+ extraembryonic ectoderm inclusion is not a transient state of all *Smad5* mutants, but represents a possible alternative consequence of a posterior amniotic ectoderm deficit in the absence of SMAD5.

Altered apoptosis, proliferation or ECM production are unlikely to cause the amniotic deficit

An amniotic ectoderm deficit could result from alterations in apoptosis or cell proliferation. TUNEL analysis revealed little cell death in mutant or control conceptuses with no evidence of increased apoptosis in mutants (**Fig. S6A**), in agreement with apoptosis-related gene sets being unaltered in mutants in GSEA. Quantification of proliferation in the ectoderm of the amniochorionic fold by phopho-histone 3 (PH3) detection revealed no significant difference in mitotic cells between control and knockout embryos (**Fig. S6A-B**).

Altered cell shape, ECM assembly and/or cell-cell and cell-matrix interactions may affect the squamous architecture and expansion of the amniotic ectoderm in mutants. GSEA analysis confirmed robust downregulation in "collagen and ECM" related gene sets in mutants (**Figs S3B-C, Table S2**). This differential expression could be due to absence of SMAD5 in amniotic ectoderm but could also reflect the relative underrepresentation of amniotic ectoderm over trapped non-amniotic tissue. We examined the spatial protein distribution of the ECM component collagen IV (ColIV). Normally, the ColIV matrix intertwined between amniotic ectoderm and mesoderm cells at E7.5 and E8.5 (**Fig. S7A-B**). In mutants, ColIV deposition seemed unaffected in regions where the amnion was a smooth, thin bilayer. ColIV was however absent from ectoderm in regions with thickened amniotic ectoderm or an aggregate, and seemed only anchored by amniotic mesoderm (**Fig. S7A-B**). Postn, an ECM protein that directly interacts with Fibronectin, ColI and ColIV (Conway et al., 2011; Horiuchi et al., 1999), had a similar distribution as ColIV in mutants (**Fig. S7C**). The differential presence of collagens and Postn in the amniotic aggregate supported amnion identity being partially affected. This may result from altered properties of the anterior amniotic ectoderm in controlling shape and stretch-ability (anterior amniotic ectoderm misdifferentiation) or inclusion of non-amniotic epiblast-derived tissue (epiblast-inclusion).

DISCUSSION

Clonal analysis of normal amnion development showed that only a few descendants of some cells in a restricted area of the early proximal anterolateral epiblast contribute to amniotic ectoderm development. These descendants expand the amnion in distinct modes. Type I cells initiate amniotic ectoderm development and, together with Type II cells, expand this tissue from the posterior (**Fig. 8A-B**). They originate in the epiblast adjacent to the extraembryonic ectoderm, which is a potent source of BMP4 and BMP8b (Ying et al. 2000; Lawson et al. 1999) and they contribute to allantois, PGCs, extraembryonic mesoderm and posterior embryonic mesoderm (Lawson and Hage 1994). Type I and II progenitors have co-descendants in exactly these posterior tissues, and all these tissues are delayed and reduced in *Smad5* mutants (Bosman et al., 2006). Type III clones contribute facultatively, from the periphery, to amniotic ectoderm, and are derived from a region (presumptive surface ectoderm) that requires BMP signalling (Madabhushi and Lacy, 2011). Strikingly, Type IV progenitors reside in the epiblast spanning the anterior midline of the extraembryonic-embryonic junction at ES+/MS, an area that is then precisely overlain by a restricted source of BMP2 in the anterior visceral endoderm (Madabhushi and Lacy 2011). Overall, the identified progenitor regions are in close proximity to BMP sources, the relationship being closest for the very restricted, sequentially present Type I and IV progenitors that generate the bulk of the amniotic ectoderm.

When relating the clonal analysis results to the *Smad5* mutant embryo analyses (**Fig. 8B-D**), the consistently delayed and posteriorized proamniotic canal closure is compatible with a posterior amniotic ectoderm deficiency resulting from undersized or delayed BMP4-dependent amniotic ectoderm founding population(s) (Type I (and II)). The inclusion of chorionic extraembryonic ectoderm in the amniotic environment of KO-SetB and some tetraploid chimeras, showed that the trailing chorionic portion of the amniochorionic fold may become trapped in the amnion at proamniotic canal closure (**Fig. 8C**).

In the majority of the mutants, the KO-SetA mutants, the phenotype seems to implicate primarily the Type IV group (**Fig. 8D**). In these mutants, the anterior extraembryonic-embryonic border is obscure, and the anterior ectoderm is non-squamous. One possibility is that the Type IV progenitor population expands normally in the amniotic ectoderm territory but fails to acquire the typical expanded squamous morphology of amniotic epithelium. Alternatively, underrepresentation of Type IV descendants is compensated by inclusion of neighbouring anterior surface ectoderm into the amniotic environment. The RNA-seq analysis did not directly support such an event as there was no major differential expression of surface ectoderm markers like e.g. *Dlx5* or *Aldh1a3* (Qu et al., 2016), however low abundant transcripts may have been underrepresented in our study. Conversely, the

persistent expression of the early epiblast marker *Fgf5* in the anterior extraembryonic-embryonic junction region of the mutants is suggestive of a stalled epiblast differentiation (atypical anterior ectoderm). In the absence of specific molecular markers of amniotic ectoderm in ES/MS embryos, the answer to whether the KO-SetA signature tissue is due to misdifferentiated Type IV descendants or atypical surface ectoderm, could potentially be obtained from prospective lineage analyses at ES+ to LS stages in *Smad5* mutants.

Further support for SMAD5 being a major signal mediator of BMP2 in the proximal anterolateral region of the embryo comes from mice that lack *Bmp2* ubiquitously or conditionally in the anterior visceral endoderm (Zhang and Bradley 1996; Madabhushi and Lacy 2011). Such embryos show defects that are reminiscent of and equally variable as those in *Smad5* mutants (Bosman et al., 2006; Chang et al., 1999) and tetraploid chimeras; *i.e.* proamniotic canal closure defects, severely impaired anterior midline epiblast tissues and ventral folding morphogenesis defects. However, an aggregate with posterior streak mesoderm potency in the anterior part of the amnion seems to form exclusively in *Smad5* mutants. This suggests that SMAD5 deficiency compromises additional BMP signalling pathways, e.g. BMP4, but potentially also BMP5 that is produced in embryonic mesoderm flanking the anterior extraembryonic-embryonic interface (Solloway and Robertson, 1999). Alternatively, intracellular non-SMAD5 cascades could be disturbed. Indeed, in cell culture experiments loss of SMAD5 can result in gain of Nodal-SMAD2/3 signalling (Pereira et al., 2012). Indications of such alterations in the *Smad5* mutants are the robust ectopic expression of *Nodal* and gain-of Nodal signalling (expression of Nodal-SMAD2/3 target genes *Lefty2, Eomes, Cripto, Wnt3*) in the non-squamous cells in anterior amniotic ectoderm (Pereira et al., 2012a) and in the KO-SetA RNA-seq results.

The chimera study showed that the amniotic aggregate is of epiblast origin, excluding that extraembryonic ectoderm inclusions (KO-SetB) transdifferentiate into an aggregate consisting of posterior streak mesoderm (KO-SetA mutants). However, the intermediate expression of selected KO-SetB and KO-SetA markers in some mutant amnion samples (8/25) is compatible with 'mixed' or variable phenotypes. Whether a mutant develops into a SetA or SetB phenotype, or 'anterior' and 'posterior' amniotic ectoderm defects co-exist, may be a stochastic event. When the amniotic ectoderm does not stretch fast enough around the time of proamniotic canal closure, the mechanical forces at the extraembryonic-embryonic interface that balance turgor in the exocoelom and (pro)amniotic cavities may 'drag' tissue from the conceptus into the amniotic ectoderm from wherever there is least resistance (as normally in type III clone behaviour). Interestingly, an extraembryonic ectoderm inclusion in the amnion has also been described for *Pagr1a* knockouts

(Kumar et al., 2014). *Pagr1a* encodes a Pax-interacting protein predominantly expressed in the chorion. Its absence results in downregulation of *Bmp2* in the anterior extraembryonic-embryonic junction.

The driving force behind the cuboidal-to-squamous transition of amniotic ectoderm still remains unclear. Interestingly, BMP-SMAD signalling has been reported as a driver of organogenesis by regulating cell shape and interpreting mechanical forces at the tissue-level (Nerurkar et al., 2017; Poduri et al., 2017; Wang et al., 2012). It is likely that the increase in turgor associated with the dynamic expansion of the exocoelomic and amniotic cavities, the folding morphogenesis of the embryo following amnion-chorion separation, and/or alterations in cell-matrix and cell-cell interactions each contribute to significant changes in cytoskeletal rearrangements. Our study relates BMP-SMAD signalling to these events in the amniotic ectoderm.

Collectively, the amnion RNA-seq approach and chimera study have shown that SMAD5 mediates spatial cues critical for the establishment of the amniotic ectoderm. The founding population of the amniotic ectoderm in mouse embryos deficient in SMAD5 is probably too small or delayed and the stalled cuboidal-to-squamous transition of anterior amniotic ectoderm does not keep pace with exocoelom expansion, hindering axial growth and ventral folding morphogenesis. The complex and variable amnion phenotypes can be attributed to SMAD5 loss-of-function affecting different progenitor populations for amniotic ectoderm. These arise sequentially from a distinct region of the anterior proximal epiblast exposed to BMP4 and BMP2 and expand amniotic ectoderm initially posteriorly and then from the anterior. Our study also supports a new role for the flexible amnion, in addition to its known protective function, one in accommodating the shaping of the embryo proper.

MATERIALS AND METHODS

Embryo culture, single cell labelling and clone plotting

[C57BL6 x CBA.Ca] F1 and F2, and some Dub:ICR, mouse (*Mus musculus*) embryos were used (**Table S5**). Terminology on embryo staging was as in (Lawson and Wilson 2016). For the nominal age at injection, embryonic day was counted with E0 being the middle of the dark period during overnight mating. 0.1 day was subtracted to allow for the developmental delay due to dissection and labelling. Culture of E6 PS stage and E6.5 ES stage embryos and the iontophoretic injection of single epiblast cells were as reported previously (Perea-Gomez et al. 2001; Lawson et al. 1991), (Beddington and Lawson 1990). In brief, clones were generated by iontophoretically injecting one epiblast cell/embryo with either a mixture of 7.4% HRP (horse radish peroxidase, EIA grade, Roche, 10814407001) and 2.6% LRDX (lysinated rhodamine dextran, M_r 10 x 10^3, Molecular Probes, D1817) or with 10% LRDX alone,

both in 0.05M KCl, using 1-3 nA depolarising current for 10-20 secs, with a duty cycle of 500 msec/sec and frequency of one second. An additional injection of 5-10 sec into an extraembryonic visceral endoderm cell in the same focal plane provided a marker clone in the same radial position as the injected epiblast cell. Embryos were cultured for one day or 1.5+ days, stained for HRP where relevant, fixed with 5% paraformaldehyde in PBS, dehydrated and cleared in BABB, when labelled cells were counted. The location and number of labelled cells were confirmed on 7 µm serial sections of the material embedded in glycol methacrylate (Technovit). PGCs were identified on the basis of their characteristic pattern of alkaline phosphatase activity, in sections of embryos labelled only with LRDX (Ginsburg et al., 1990; Lawson and Hage, 1994).

Clonal descendants in the amniotic ectoderm were plotted on an appropriate template using information from the whole mount and sections to normalize the plot. Amnion templates were derived from 3D embryo reconstructions in the eMouseAtlas (Armit et al., 2017), specifically EMA:224 (TS 10b, LSEB/EPHF), EMA:17 (TS 11, LPHF/EHF), EMA:220 (TS 12a, 2S), and EMA:218 (TS 12b, 5S). Templates were created from measurements over the surface of the amnion in both sagittal and frontal orientation. Because of the extreme curvature of the amnion by the 5S stage, the 2D template for this stage is a compromise between the linear dimensions over the surface and the shorter periphery of the base of a dome. Template dimensions were adjusted for 20% shrinkage during histological processing of the embryos used in the eMouseAtlas.

Smad5 mutant mouse strain, microdissection and genotyping

Smad5-deficient mouse embryos (within decidua or isolated) from heterozygous *Smad5*$^{-/+}$ crosses (*Smad5*^{tm1Zuk})(Chang et al., 1999) of mixed C57BL/6J x CBA background were collected in ice-cold PBS at E7.5-E8.5. Amnion was stepwise microsurgically isolated from EPHF to 2S stage embryos using tungsten needles as shown in **Fig. 4C-D**, and frozen on dry ice. PCR genotyping was performed on left-over embryonic material. For genotyping of embryos sectioned within the decidua, side sections were mounted on PALM membrane slides (Zeiss 415190-9041-000), stained with cresyl violet and subjected to Laser Capture Microdissection (LCM) on PALM MicroBeam laser capture system (Zeiss) to isolate embryonic tissue for genotyping. DNA for PCR was isolated after on-cap lysis in LCM lysis buffer (0.5M EDTA pH 8.0, 1M Tris pH 8.0 and Igepal CA-630). Sex was determined by Jarid1c/Jarid1d and Sry/IL3 PCR (**Table S6**). In all experiments, stage-matched Smad5$^{-/+}$ or Smad5$^{+/+}$ littermates were used as controls to Smad5$^{-/-}$ embryos. All animal experiments were approved by the ethical commission of KU

Leuven (P097/2008; P077/2014; P251/2014).

Quantitative reverse-transcription PCR (RT-qPCR)

Primers for RT-qPCR on cDNA from single amnion samples (**Table S6**) were designed in maximal proximity to the 3' ends of target transcripts, to compensate for the potential 3' bias that might be generated during amplification (see "Single amnion cDNA amplification"). Samples were processed on LightCycler480 Real-Time PCR System with LightCycler 480 SYBRGreen I Master mix (Roche, 4707516001) in technical duplicates. Reference genes for amniotic tissue were chosen using GeNorm. For the analysis in **Fig. 5D**, expression was normalized to two reference genes - Gapdh and Psmd4, using the ΔΔCt method and qbase+ software (Biogazelle). For the analysis shown in **Fig. S3A**, expression was normalized to Psmd4, and presented with the ΔCt method which reflects the Ct difference between the reference and the test transcript (in **Fig. S3A**, the higher ΔCt, the higher the expression).

Single amnion cDNA amplification

cDNA for RT-qPCR and RNA-seq was prepared from individual E7.5 amnions and amplified following adaptation of a procedure originally designed for RNA-seq of single-cells (Tang et al., 2009) on the SOLiD platform ("Double stranded cDNA synthesis from a single cell", Applied Biosystems demonstrated protocol). Briefly, reverse transcription and second-strand cDNA synthesis was performed in the sample lysate without RNA isolation, using SuperScript III Reverse Transcriptase (Invitrogen) and poly-dT universal primers. This was followed by two rounds of PCR amplification (18 and 12 cycles, respectively) and column purifications (QIAquick, QIAGEN) generating up to 3 kb coverage at the 3' end of all poly-adenylated transcripts. The resulting cDNA was used for RT-qPCR and RNA-seq. The cDNA yield for the 12 RNA-seq samples is shown in **Table S1**.

Whole transcriptome sequencing and bioinformatics analysis

Between 30-60 million reads were generated per library; 20%-27% of them mapped uniquely to the genome (**Table S1**). Raw colorspace reads were mapped to the mouse genome GRCm38.83 with TopHat2 software (v2.1.1)(Kim et al., 2013; Trapnell et al., 2009) using colorspace compatible parameters: Bowtie 1 (v1.1.2.0), --color --quals and coverage-search algorithm. Transcript coordinates were extracted from the Genome Reference Center reference annotation with Gffread from the Cufflinks v2.1.1 suite and merged to gene coordinates with mergeBed from the Bedtools v2.17.0 toolkit)(Kim et al., 2013; Quinlan and Hall, 2010; Trapnell et al., 2011). GC content and gene length

were derived from the gene coordinates. The numbers of aligned reads per gene were summarized using featureCounts v1.5.3 with parameters '-Q 0 -s 0 -t exon -g gene id' (Liao et al., 2014). We removed 22,528 genes for which all samples had less than 1 count-per-million. As such, we continued with raw counts for 16,033 genes.

Raw counts were imported in R package DESeq2 1.18.1 (Love et al., 2014) for library size normalization and differential expression analyses. The counts were subjected to variance stabilizing transformation (VST) (Anders and Huber 2010). The variance normalized counts were used for gene expression visualization and clustering. Clustering of all 12 samples was performed by Principal Component Analysis (PCA). In DESeq2, a negative binomial generalized linear model (GLM) was fitted against the normalized counts. Differential expression was tested for with a Wald statistical test, also implemented in the DESeq2 package. The resulting p-values were corrected for multiple testing with Benjamini-Hochberg to control the false discovery rate (FDR). Differentially expressed genes were further filtered using FDR ≤ 0.05 and |log2 FC| ≥1. Expression heat maps were generated in MultiExperiment Viewer (MeV) using VST values. GSEA analysis is described in Supplementary Materials and Methods.

Immunohistochemistry, TUNEL assay and whole mount *in situ* hybridization
Embryos and decidua were fixed overnight in 4% paraformaldehyde in PBS, embedded in paraffin and sectioned at 6 μm. Fixed chimeric embryos were pre-embedded in 1.5% agarose prior to paraffin embedding and sectioning. Fluorescent and chromogenic antibody stainings were performed on an automated platform (Ventana Discovery, Ventana Medical Systems) or manually using standard procedures. We used antibodies raised against: Oct3/4 (1:100, ab19857), Eomes (1:250, ab23345), Collagen IV (1:100, ab6586), phospho-Histone 3 (1:100, ab5176) and GFP (1:100, ab13970) from Abcam; and Elf5 (1:40, sc-9645) and periostin (1:100, sc-67233) from Santa Cruz Biotechnology. Differently labelled secondary antibodies raised in donkey or goat were used (Jackson ImmunoResearch, 1:300). Omitting the primary antibody served as negative control. Nuclei were counterstained with DAPI (1:1000, InVitrogen D3571) or haematoxylin. TUNEL assay was performed using a Fluorescein In Situ Cell Death Detection kit (Roche) according to manufacturer's instructions. Proliferation data was statistically analysed with Prims 6 software (GraphPad). The non-parametric Mann-Whitney U-test was used for comparisons of the two groups.

Whole mount *in situ* hybridisation was performed as previously described (Pereira et al., 2011). The *Fgf5* cDNA template used for riboprobe synthesis and digoxigenin-labeling was generated by PCR (**Table S6).** Probe hybridisation was at 60°C.

Tetraploid complementation assay and generation of chimeric embryos

Chimeric embryos were produced as described (Eakin and Hadjantonakis 2006). Briefly, tetraploidy was achieved by electrofusion of 2-cell stage CD1 embryos. Wild-type and *Smad5* knockout mouse ESCs (Bosman et al., 2006) were transfected with lentivirus containing eGFP gene under the control of elongation factor-1 alpha promoter. Two tetraploid zona pellucida-free morula embryos were aggregrated with GFP+ ESCs to produce *Smad5$^{-/-}$;GFP+* ESC<> 4n WT and *WT;GFP+* ESC<> 4n WT chimeras, respectively knockout and WT chimeras. Blastocysts were transferred into the uteri of pseudo-pregnant females. Embryos were microdissected, imaged for GFP fluorescence and fixed. In total, 35 knockout and 5 WT chimeras were embedded in agarose and paraffin. Sections were subjected to immunofluorescence against GFP.

DATA AVAILABILITY

Data availability of the RNA-seq analysis: GEO
https://www.ncbi.nlm.nih.gov/geo/query/acc.cgi?acc=GSE99211 token srcrgokcfxqrbkh.

REFERENCES

Armit, C., Richardson, L., Venkataraman, S., Graham, L., Burton, N., Hill, B., Yang, Y. and Baldock, R. A. (2017). eMouseAtlas: An atlas-based resource for understanding mammalian embryogenesis. *Developmental biology* **423**, 1–11.

Arnold, S. J., Hofmann, U. K., Bikoff, E. K. and Robertson, E. J. (2008). Pivotal roles for eomesodermin during axis formation, epithelium-to-mesenchyme transition and endoderm specification in the mouse. *Development* **135**, 501–511.

Beddington, R.S.P & Lawson, K. A. (1990). Clonal Analysis of Cell Lineage. In *Postimplantation Mammalian Embryos: a Practical Approach* (ed. D.L., C. A. J. & C.), pp. 267–316. Oxford: IRL Press.

Bosman, E. A., Lawson, K. A., Debruyn, J., Beek, L., Francis, A., Schoonjans, L., Huylebroeck, D. and Zwijsen, A. (2006). Smad5 determines murine amnion fate through the control of bone morphogenetic protein expression and signalling levels. *Development (Cambridge, England)* **133**, 3399–3409.

Cajal, M., Lawson, K. A., Hill, B., Moreau, A., Rao, J., Ross, A., Collignon, J., Camus, A., Acampora, D., Merlo, G. R., et al. (2012). Clonal and molecular analysis of the prospective anterior neural boundary in the mouse embryo. *Development (Cambridge, England)* **139**, 423–36.

Cajal, M., Creuzet, S. E., Papanayotou, C., Sabéran-Djoneidi, D., Chuva de Sousa Lopes, S. M., Zwijsen, A., Collignon, J. and Camus, A. (2014). A conserved role for non-neural ectoderm cells in early neural development. *Development (Cambridge, England)* **141**, 4127–38.

Chang, H., Huylebroeck, D., Verschueren, K., Guo, Q., Matzuk, M. M. and Zwijsen, A. (1999). Smad5 knockout mice die at mid-gestation due to multiple embryonic and extraembryonic defects. *Development (Cambridge, England)* **126**, 1631–1642.

Ciruna, B. G. and Rossant, J. (1999). Expression of the T-box gene Eomesodermin during early mouse development. *Mechanisms of Development* **81**, 199–203.

Conway, S. J., Doetschman, T. and Azhar, M. (2011). The inter-relationship of periostin, TGF beta, and BMP in heart valve development and valvular heart diseases. *TheScientificWorldJournal* **11**, 1509–1524.

de Melo Bernardo, A. and Chuva de Sousa Lopes, S. M. (2014). The Involvement of the Proamnion

in the Development of the Anterior Amnion Fold in the Chicken. *PLoS ONE* **9**, e92672.

Dobreva, M. P., Lhoest, L., Pereira, P. N. G., Umans, L., Camus, A., Chuva de Sousa Lopes, S. M. and Zwijsen, A. (2012). Periostin as a Biomarker of the Amniotic Membrane. *Stem Cells International* **2012**, 1–10.

Donnison, M., Beaton, A., Davey, H. W., Broadhurst, R., L'Huillier, P. and Pfeffer, P. L. (2005). Loss of the extraembryonic ectoderm in Elf5 mutants leads to defects in embryonic patterning. *Development (Cambridge, England)* **132**, 2299–308.

Downs, K. M. (2008). Systematic localization of oct-3/4 to the gastrulating mouse conceptus suggests manifold roles in mammalian development. *Developmental Dynamics* **237**, 464–475.

Eakin, G. S. and Hadjantonakis, A.-K. (2006). Production of chimeras by aggregation of embryonic stem cells with diploid or tetraploid mouse embryos. *Nature protocols* **1**, 1145–53.

Egea, J., Erlacher, C., Montanez, E., Burtscher, I., Yamagishi, S., Hess, M., Hampel, F., Sanchez, R., Rodriguez-Manzaneque, M. T., Bosl, M. R., et al. (2008). Genetic ablation of FLRT3 reveals a novel morphogenetic function for the anterior visceral endoderm in suppressing mesoderm differentiation. *Genes & Development* **22**, 3349–3362.

Ginsburg, M., Snow, M. and McLaren, A. (1990). Primordial germ cells in the mouse embryo during gastrulation. *Development* **110**, 521–528.

Horiuchi, K., Amizuka, N., Takeshita, S., Takamatsu, H., Katsuura, M., Ozawa, H., Toyama, Y., Bonewald, L. F. and Kudo, A. (1999). Identification and Characterization of a Novel Protein, Periostin, with Restricted Expression to Periosteum and Periodontal Ligament and Increased Expression by Transforming Growth Factor β. *Journal of Bone and Mineral Research* **14**, 1239–1249.

Horn, T. and Panfilio, K. A. (2016). Novel functions for *Dorsocross* in epithelial morphogenesis in the beetle *Tribolium castaneum*. *Development* **143**, 3002–3011.

Imuta, Y., Koyama, H., Shi, D., Eiraku, M., Fujimori, T. and Sasaki, H. (2014). Mechanical control of notochord morphogenesis by extra-embryonic tissues in mouse embryos. *Mechanisms of Development* **132**, 44–58.

Inai, K., Norris, R. A., Hoffman, S., Markwald, R. R. and Sugi, Y. (2008). BMP-2 induces cell migration and periostin expression during atrioventricular valvulogenesis. *Developmental Biology* **315**,

383–396.

Katagiri, T. and Watabe, T. (2016). Bone Morphogenetic Proteins. *Cold Spring Harbor Perspectives in Biology* **8**, a021899.

Kim, D., Pertea, G., Trapnell, C., Pimentel, H., Kelley, R. and Salzberg, S. L. (2013). TopHat2: Accurate alignment of transcriptomes in the presence of insertions, deletions and gene fusions. *Genome Biology* **14**, R36.

Kinder, S. J., Tsang, T. E., Wakamiya, M., Sasaki, H., Behringer, R. R., Nagy, a and Tam, P. P. (2001). The organizer of the mouse gastrula is composed of a dynamic population of progenitor cells for the axial mesoderm. *Development (Cambridge, England)* **128**, 3623–3634.

Kumar, A., Lualdi, M., Loncarek, J., Cho, Y.-W., Lee, J.-E., Ge, K. and Kuehn, M. R. (2014). Loss of function of mouse Pax-Interacting Protein 1-associated glutamate rich protein 1a (Pagr1a) leads to reduced Bmp2 expression and defects in chorion and amnion development. *Developmental Dynamics* **243**, 937–947.

Lawson, K. A. and Hage, W. J. (1994). Clonal analysis of the origin of primordial germ cells in the mouse. *Ciba Foundation symposium* **182**, 68-84-91.

Lawson, K. A., Meneses, J. J. and Pedersen, R. A. (1991). Clonal analysis of epiblast fate during germ layer formation in the mouse embryo. *Development (Cambridge, England)* **113**, 891–911.

Lawson, K. A., Dunn, N. R., Roelen, B. A., Zeinstra, L. M., Davis, A. M., Wright, C. V, Korving, J. P. and Hogan, B. L. (1999). Bmp4 is required for the generation of primordial germ cells in the mouse embryo. *Genes & development* **13**, 424–36.

Lawson, K. A., Wilson, V. A. (2016). Revised Staging of Mouse Development Before Organogenesis. In *Kaufman's Atlas of Mouse Development Supplement* (ed. Baldock, R.), Bard, J.), Davidson, D. R.), and Morris-Kay, G.), pp. 51–64. Elsevier.

Li, L., Liu, C., Biechele, S., Zhu, Q., Song, L., Lanner, F., Jing, N. and Rossant, J. (2013). Location of transient ectodermal progenitor potential in mouse development. *Development* **140**, 4533–4543.

Liao, Y., Smyth, G. K. and Shi, W. (2014). FeatureCounts: An efficient general purpose program for assigning sequence reads to genomic features. *Bioinformatics* **30**, 923–930.

Love, M. I., Huber, W. and Anders, S. (2014). Moderated estimation of fold change and dispersion

for RNA-seq data with DESeq2. *Genome Biology* **15**, 1–21.

Madabhushi, M. and Lacy, E. (2011). Anterior visceral endoderm directs ventral morphogenesis and placement of head and heart via BMP2 expression. *Developmental cell* **21**, 907–19.

Menon, R. and Richardson, L. S. (2017). Preterm prelabor rupture of the membranes: A disease of the fetal membranes. *Seminars in Perinatology* **41**, 409–419.

Mesnard, D. and Constam, D. B. (2010). Imaging proprotein convertase activities and their regulation in the implanting mouse blastocyst. *The Journal of cell biology* **191**, 129–39.

Nerurkar, N. L., Mahadevan, L. and Tabin, C. J. (2017). BMP signaling controls buckling forces to modulate looping morphogenesis of the gut. *Proceedings of the National Academy of Sciences* **114**, 2277–2282.

Opitz, J. M., Johnson, D. R. and Gilbert-Barness, E. F. (2015). ADAM "sequence" part II: Hypothesis and speculation. *American Journal of Medical Genetics Part A* **167**, 478–503.

Perea-Gomez, A., Lawson, K. A., Rhinn, M., Zakin, L., Brûlet, P., Mazan, S. and Ang, S. L. (2001). Otx2 is required for visceral endoderm movement and for the restriction of posterior signals in the epiblast of the mouse embryo. *Development (Cambridge, England)* **128**, 753–65.

Pereira, P. N. G., Dobreva, M. P., Graham, L., Huylebroeck, D., Lawson, K. A. and Zwijsen, A. N. (2011). Amnion formation in the mouse embryo: the single amniochorionic fold model. *BMC developmental biology* **11**, 48.

Pereira, P. N., Dobreva, M. P., Maas, E., Cornelis, F. M., Moya, I. M., Umans, L., Verfaillie, C. M., Camus, A., de Sousa Lopes, S. M., Huylebroeck, D., et al. (2012). Antagonism of Nodal signaling by BMP/Smad5 prevents ectopic primitive streak formation in the mouse amnion. *Development* **139**, 3343–3354.

Poduri, A., Raftrey, B., Chang, A. H., Rhee, S., Van, M. and Red-Horse, K. (2017). Endothelial cells respond to the direction of mechanical stimuli through SMAD signaling to regulate coronary artery size. *Development* dev.150904.

Qu, Y., Zhou, B., Yang, W., Han, B., Yu-Rice, Y., Gao, B., Johnson, J., Svendsen, C. N., Freeman, M. R., Giuliano, A. E., et al. (2016). Transcriptome and proteome characterization of surface ectoderm cells differentiated from human iPSCs. *Scientific Reports* **6**, 32007.

Quinlan, A. R. and Hall, I. M. (2010). BEDTools: A flexible suite of utilities for comparing genomic

features. *Bioinformatics* **26**, 841–842.

Rafiqi, A. M., Park, C.-H., Kwan, C. W., Lemke, S. and Schmidt-Ott, U. (2012). BMP-dependent serosa and amnion specification in the scuttle fly Megaselia abdita. *Development* **139**, 3373–3382.

Sasaki, K., Nakamura, T., Okamoto, I., Yabuta, Y., Iwatani, C., Tsuchiya, H., Seita, Y., Nakamura, S., Shiraki, N., Takakuwa, T., et al. (2016). The Germ Cell Fate of Cynomolgus Monkeys Is Specified in the Nascent Amnion. *Developmental Cell* **39**, 169–185.

Schmidt, W. (1992). The amniotic fluid compartment: the fetal habitat. *Advances in anatomy, embryology, and cell biology* **127**, 1–100.

Shao, Y., Taniguchi, K., Gurdziel, K., Townshend, R. F., Xue, X., Yong, K. M. A., Sang, J., Spence, J. R., Gumucio, D. L. and Fu, J. (2016). Self-organized amniogenesis by human pluripotent stem cells in a biomimetic implantation-like niche. *Nature materials*.

Solloway, M. J. and Robertson, E. J. (1999). Early embryonic lethality in Bmp5;Bmp7 double mutant mice suggests functional redundancy within the 60A subgroup. *Development (Cambridge, England)* **126**, 1753–1768.

Tang, F., Barbacioru, C., Wang, Y., Nordman, E., Lee, C., Xu, N., Wang, X., Bodeau, J., Tuch, B. B., Siddiqui, A., et al. (2009). mRNA-Seq whole-transcriptome analysis of a single cell. *Nature Methods* **6**, 377–382.

Tomás, A. R., Certal, A. C. and Rodríguez-León, J. (2011). FLRT3 as a key player on chick limb development. *Developmental Biology* **355**, 324–333.

Trapnell, C., Pachter, L. and Salzberg, S. L. (2009). TopHat: discovering splice junctions with RNA-Seq. *Bioinformatics (Oxford, England)* **25**, 1105–11.

Trapnell, C., Williams, B. a, Pertea, G., Mortazavi, A., Kwan, G., van Baren, M. J., Salzberg, S. L., Wold, B. J. and Pachter, L. (2011). Transcript assembly and abundance estimation from RNA-Seq reveals thousands of new transcripts and switching among isoforms. *Nature Biotechnology* **28**, 511–515.

Wang, Y.-K., Yu, X., Cohen, D. M., Wozniak, M. A., Yang, M. T., Gao, L., Eyckmans, J. and Chen, C. S. (2012). Bone Morphogenetic Protein-2-Induced Signaling and Osteogenesis Is Regulated by Cell Shape, RhoA/ROCK, and Cytoskeletal Tension. *Stem Cells and Development* **21**, 1176–1186.

**Yang, X., Castilla, L. H., Xu, X., Li, C., Gotay, J., Weinstein, M., Liu, P. P. and Deng, C. X.** (1999). Angiogenesis defects and mesenchymal apoptosis in mice lacking SMAD5. *Development* **126**,.

Ying, Y. and Zhao, G.-Q. (2001). Cooperation of Endoderm-Derived BMP2 and Extraembryonic Ectoderm-Derived BMP4 in Primordial Germ Cell Generation in the Mouse. *Developmental Biology* **232**, 484–492.

Ying, Y., Liu, X.-M., Marble, A., Lawson, K. A. and Zhao, G.-Q. (2000). Requirement of *Bmp8b* for the Generation of Primordial Germ Cells in the Mouse. *Molecular Endocrinology* **14**, 1053–1063.

Zhang, H. and Bradley, A. (1996). Mice deficient for BMP2 are nonviable and have defects in amnion/chorion and cardiac development. *Development (Cambridge, England)* **122**, 2977–86.
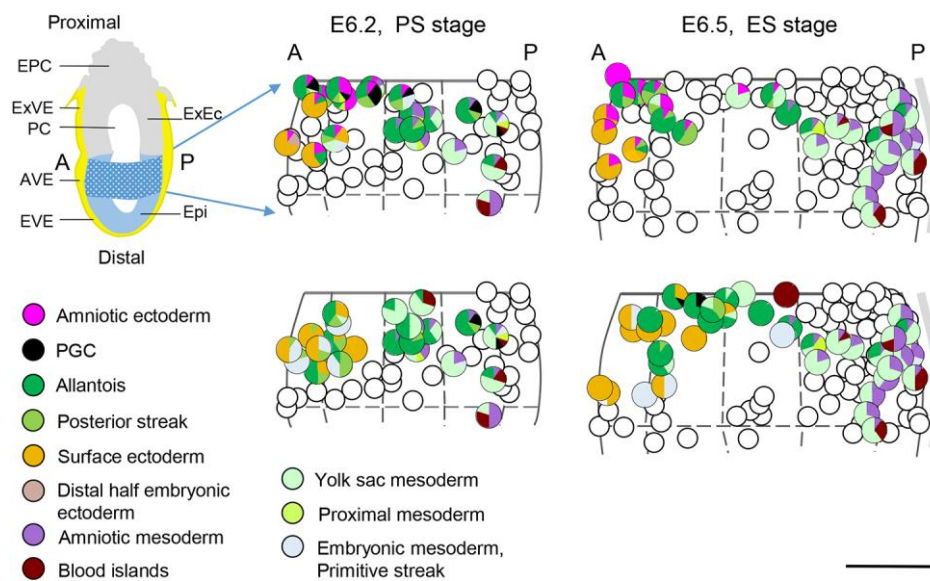
Figure 1. Amnion fate map

Fate maps of amniotic ectoderm and amniotic mesoderm. Top left: cartoon of a midsagittal section of an E6.2, prestreak stage (PS) embryo. The proximal half of the epiblast cup (blue-pattern) is expanded in the right panels and projected on the sagittal midline of PS and ES (early streak) stages. Left and right halves of the epiblast are superimposed. Half the circumference of the normalised epiblast is flattened and fitted to its diameter (D), i.e $\pi D/2$ is reduced to D. The primitive streak is represented by a grey stripe. The composition (to the nearest 10%) of clones contributing to amnion is shown as pie charts at the positions of clone initiation in the two upper panels. Clones not contributing to the amnion are represented by empty circles. Lower panel: Composition of the clones not contributing to amniotic ectoderm in the same region as in the upper panel. Clones contributing to amniotic ectoderm are nor represented for clarity. Scale bar plotted figures: 50 μm. A: anterior; AVE: anterior visceral endoderm; Epi: epiblast; EPC: ectoplacental cone; EVE: embryonic visceral endoderm; ExEc: extraembryonic ectoderm; ExVE: extraembryonic visceral endoderm; P: posterior; PC: proamniotic cavity.
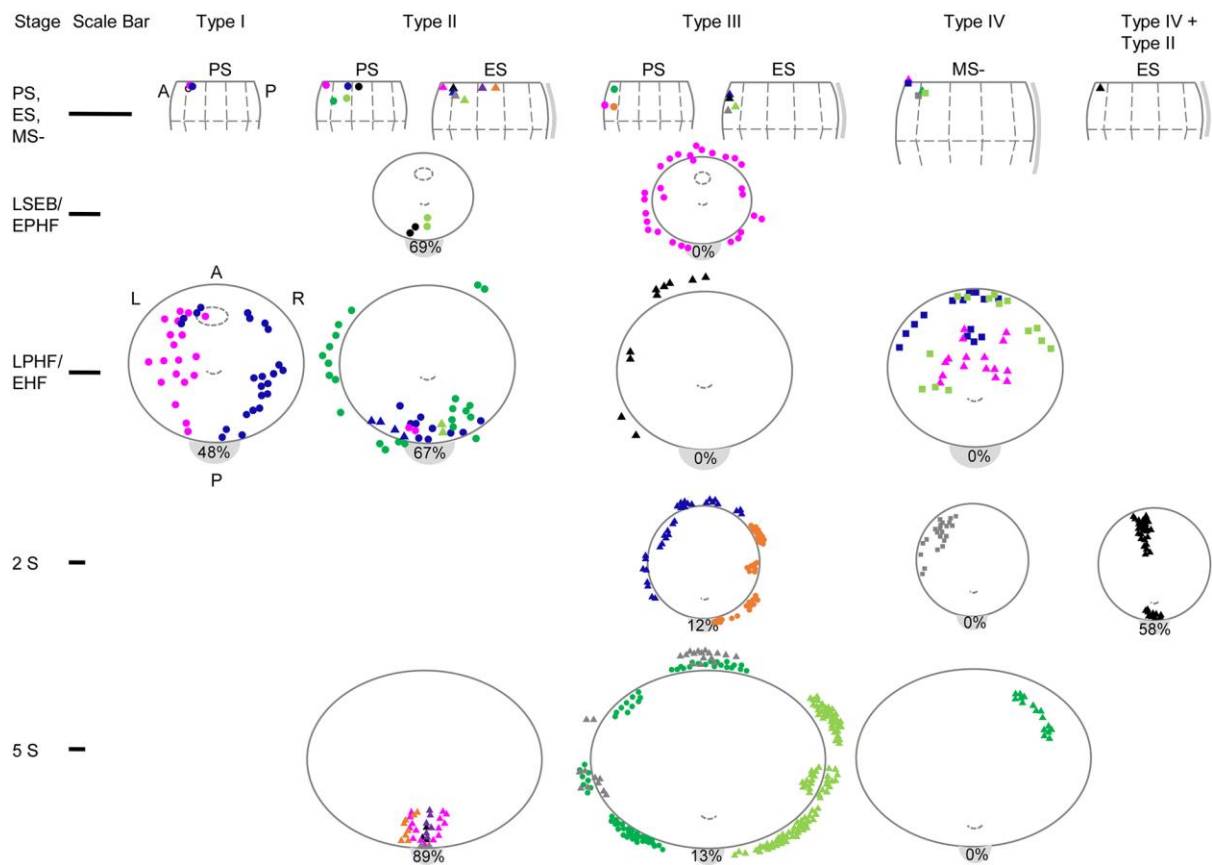
Figure 2. Spread of clone descendants in amniotic ectoderm

Clonal spread in amniotic ectoderm and associated surface ectoderm. Each clone within a Type is identified by a colour/shape combination (**Table 1**). Top row: the positions of clone progenitors are plotted, as in **Fig. 1**, on scaled representations of the proximal half of the epiblast at different initial stages (PS, ES and MS-). Scale bar: 100 µm. The top edge of the diagram is at the junction with the apposing extraembryonic (prechorionic) ectoderm. The position of the progenitor of the unplotted Type I PS clone #3 is shown as an empty circle. Lower rows: the view of clone distribution in the amniotic ectoderm (ellipse, unbroken line) is from dorsal with anterior (A) at the top. The projected position of the closing/closed proamniotic canal and node is respectively indicated by an ellipse (broken line) and an arc (broken line). Cells plotted outside the amnion are in the adjacent non-neural ectoderm (mainly surface ectoderm). The number in the grey crescent at the posterior edge of the amnion is the total number of extraembryonic mesoderm and posterior streak cells in the clones expressed as a percentage of the total labelled cells in the embryos contributing to the plot. Clones #2 (Type I, dark blue), #17 (Type III, dark blue) and #27 (Type IV, light green) are shown in LR mirror image to reduce overlapping in display.
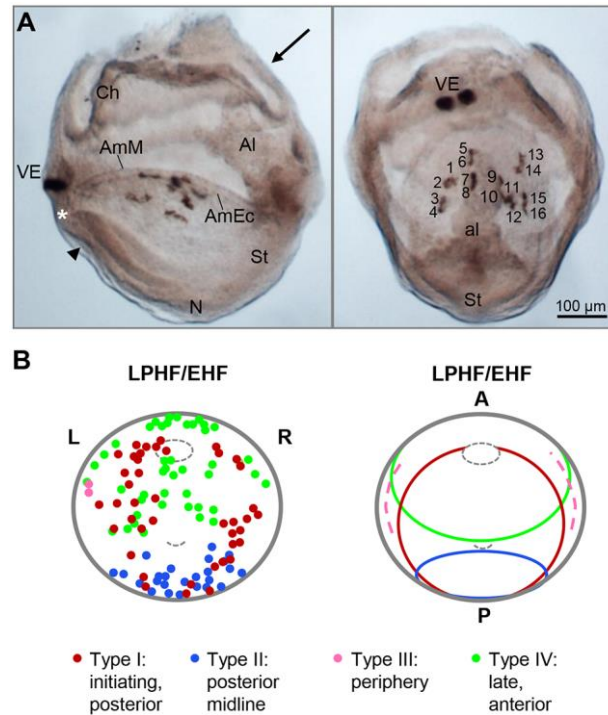
Figure 3. Illustration and summary of amniotic ectoderm clones

(A) Lateral view, anterior facing left, and posteriodorsal view (indicated by arrow in lateral view) of a mouse embryo with labelled Type IV clone (#23) in the amniotic ectoderm (**Table 1, Fig. 2**). The clone was initiated close to the midline at the extraembryonic-embryonic junction (**Fig.2**), as indicated by the VE marker clone. As this is a pure clone, there is no supporting evidence about the time of entry of descendants into the amniotic ectoderm. The pattern of four files of four cells (1-4)(5-8)(9-12)(13-16) oriented A-P indicates that the progenitor divided twice before all four descendants left the periphery of the amniotic ectoderm during the same cell cycle and went through two additional cycles of oriented cell division. Two other Type IV clones (#24 and #27) indicate that cells may divide once or twice at the anterior periphery while releasing descendants to start populating the anterior amniotic ectoderm. The asterisk and arrowhead mark the amniotic ectoderm/embryonic ectoderm junction and the incipient foregut pocket respectively. Scale bar: 100 μm.

(B) Combined distribution (left) of the four types of amniotic ectoderm clones (**Fig. 2**) in a LPHF/EHF amnion, and simplified territories (right). Anterior (A) to the top. The projected position of the closed PAC and node are respectively indicated by a small ellipse and arc (broken lines). Type I descendants initiate the primordium and establish the amniotic ectoderm posterior to the anterior separation point, whereas Type II descendants populate the most posterior midline subregion. The lineage-

restricted Type IV descendants produce the anterior-most amniotic ectoderm, and also contribute to the already established Type I territory. Type III descendants expand the amnion only at the periphery. Al: allantois; AmEc: amniotic ectoderm; AmM: amniotic mesoderm; Ch: chorion; N: node; St: streak; PAC: proamniotic canal; VE: visceral endoderm.
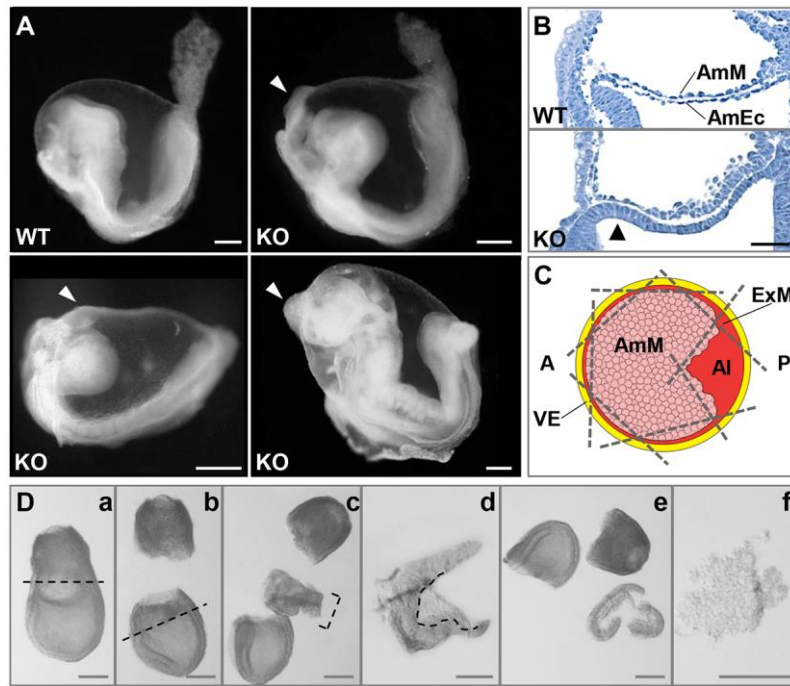
Figure 4. Phenotype of *Smad5* mutants and amnion microdissection procedure

(A) Appearance of early somite stage wild-type (WT) and *Smad5* knockout (KO) embryos. The mutant amnion contains an anteriorly localized tissue aggregate (arrowhead). Scale bar: 200 µm.

(B) Longitudinal sections of E7.5 late pre-headfold (LPHF) stage WT and *Smad5* knockout embryos stained with haematoxylin. Amniotic ectoderm (AmEc) is thickened in mutants (arrowhead). Scale bar: 50 µm. AmM: amniotic mesoderm.

(C) Scheme of a dorsal view of an amnion positioned to trim it free (see D) from neighbouring tissues; broken lines represent cuts. Al: allantoic bud; AmM: amniotic mesoderm; ExM: extraembryonic mesoderm; VE: visceral endoderm. Anterior to the left.

(D) Amnion microdissection procedure for an E7.5 LPHF embryo. Following removal of the proximal (**a**) and distal (**b**) parts of the conceptus (cuts at the broken lines), the extraembryonic-embryonic junction region (bracket in **c**) is flipped 90° and the borders and allantoic bud are trimmed from the amniotic tissue (**d**). The remaining of the conceptus (**e**) and the isolated amniotic tissue (**f**) are respectively used for genotyping and transcriptome analysis. Scale bar: 200 µm.
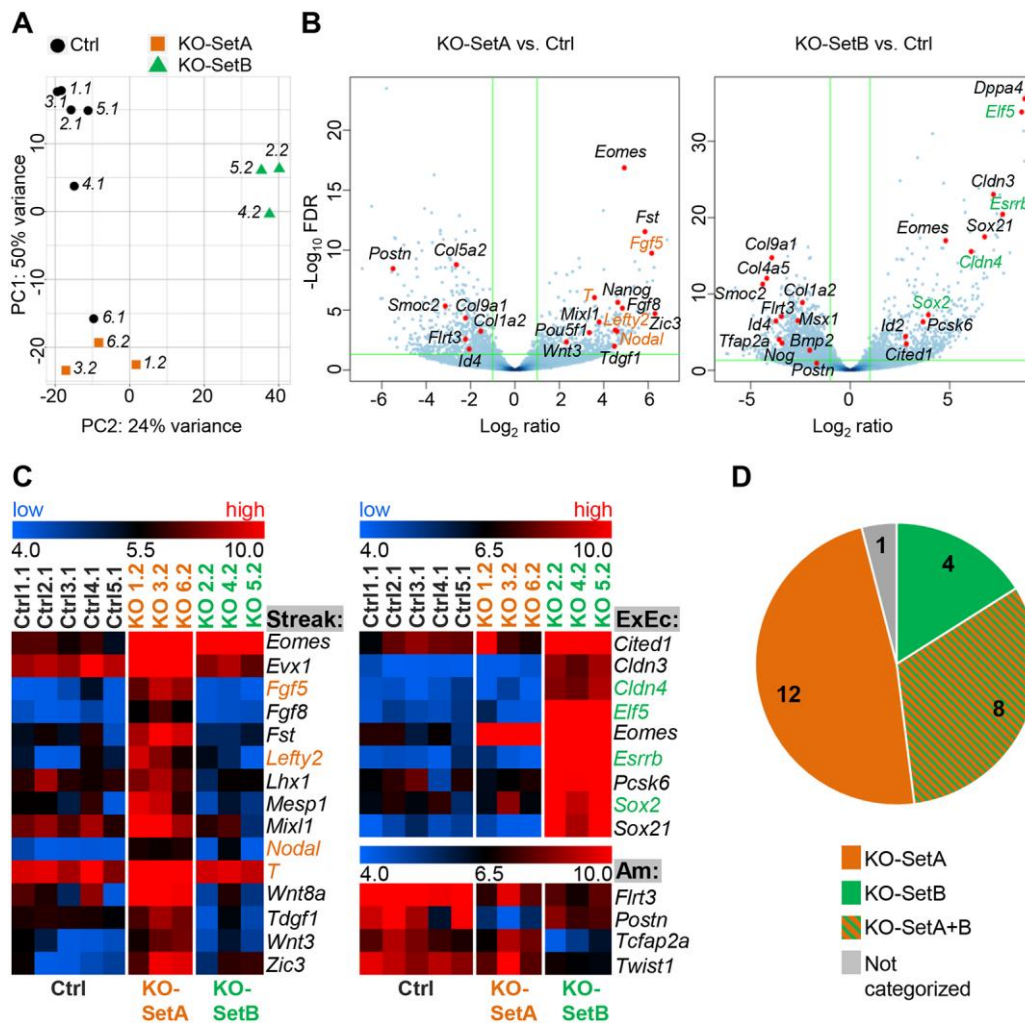
Figure 5. Differential expression analysis shows two sets of mutants with distinct signatures

(A)   Clustering of control (ctrl) and *Smad5* mutant (KO) amnion samples (details on identity tags of samples: **Table S1**) by Principal Component Analysis (PCA). The KO samples robustly segregated into two distinct groups.

(B)   Volcano plots showing the DESeq2-estimated log2-ratios versus the significance as the negative log10 adjusted p-value (FDR). Green lines correspond to the used thresholds on the FDR (<0.05) and on the log Fold Change (<-1 and >1).

(C)   Expression heat maps for selected transcripts. Scale: variance stabilized values from minimum to maximum limits of expression values. The mid-values represents the median. Streak/mesoderm markers are enriched in KO-SetA, and extraembryonic ectoderm markers (ExEc) are enriched in KO-SetB.

(D) Independent validation of RNA-seq findings. Distribution of mutant expression signatures among 25 littermate knockout/control pair amnion samples based on RT-qPCR for the KO-SetA markers *Nodal, Lefty2, T* and *Fgf5* (orange) and KO-SetB markers *Cldn4, Elf5, Esrrb,* and *Sox2* (green). A

knockout was considered to belong to a particular set if it overexpressed (> 3-fold) at least 2 of the set markers and not more than 1 marker of the other set. Knockouts with mixed signature (KO-SetA + KO-SetB) overexpressed 2 or more markers of each set. Non-categorized samples are in grey.
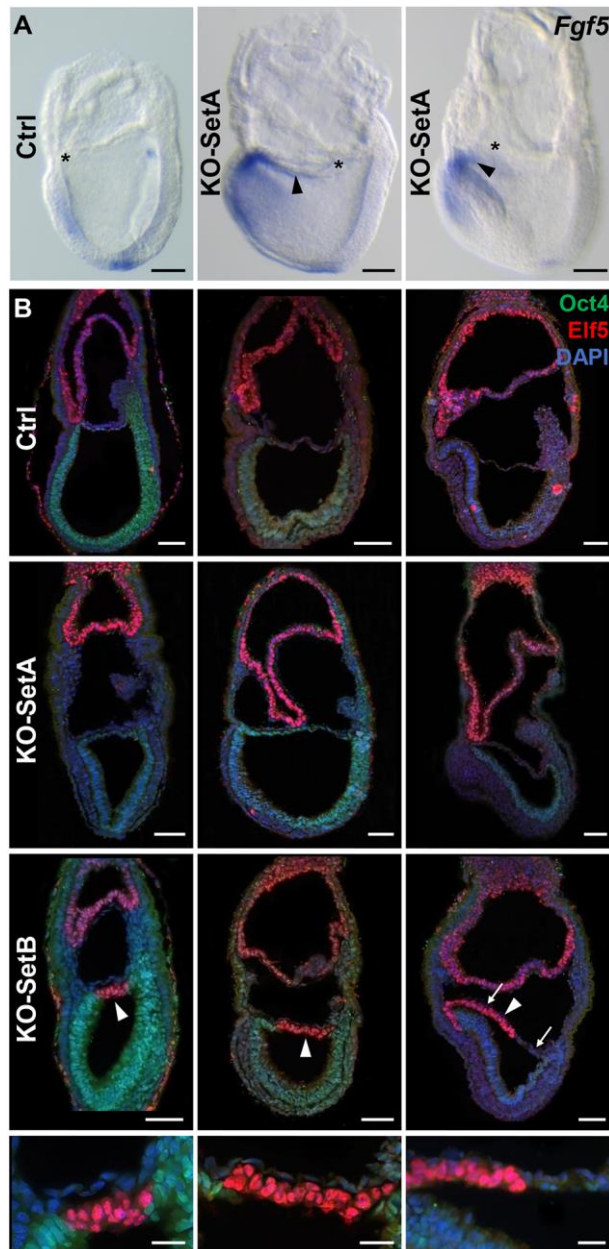
Figure 6. Ectopic presence of the epiblast marker *Fgf5* and the extraembryonic marker Elf5 in the mutant amnion

(A) In situ hybridisation of control (EPHF) and two *Smad5* knockout (EHF) embryos for *Fgf5*, a KO-SetA enriched transcript. The *Fgf5*-positive segment had a variable extension in the mutant amniotic ectoderm (KO-SetB embryos, arrowheads). The anterior separation point (asterisk), where the proamniotic canal closes and amnion and chorion separate, shifted posteriorly in mutants. Am: amnion; Ch: chorion. Scale bar: 100 μm.

(B) Longitudinal sections of control and *Smad5* knockout embryos stained with anti-Oct4/Pou5f1 and anti-Elf5 antibodies. Oct4 is present in amnion and Elf5 in chorion in control embryos and in 80% of *Smad5* knockout embryos (KO-SetA embryos), while 20% of the mutants have an Oct4-negative,

Elf5-positive segment in the amnion (KO-SetB embryos, arrowheads). Magnifications of these areas are shown. Magnified region in the lower right embryo is bracketed by arrows. Scale bars: 75 µm or 25 µm (magnifications).
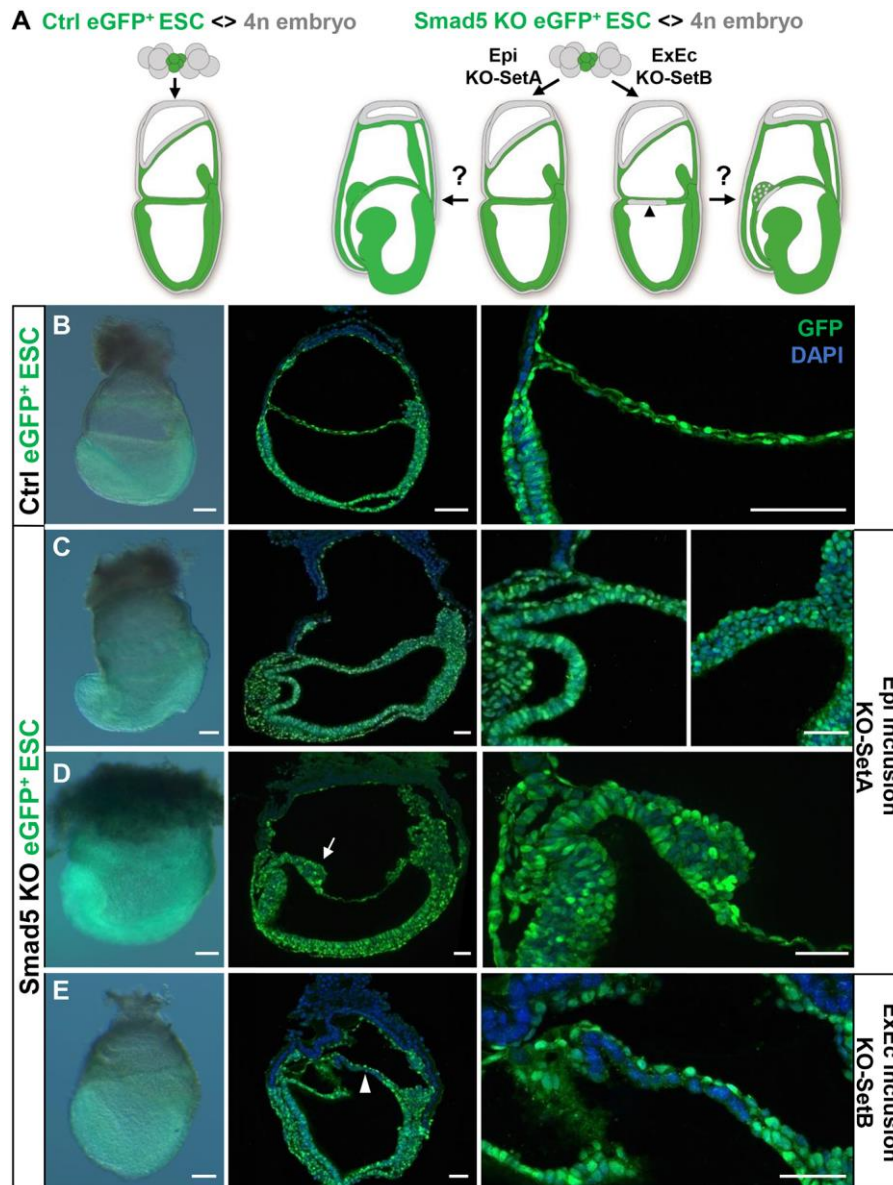
Figure 7. Tetraploid chimera production confirms two separate amnion defects in *Smad5* mutants

(**A**) Morula aggregation of control *GFP+ ESC <> 4n WT* and *Smad5⁻ᐟ⁻;GFP+ ESC <> 4n WT* assays with (potential) outcome. The mutant amnion can be completely epiblast (Epi) derived or can contain an extraembryonic ectoderm (ExEc) inclusion (arrowhead). The latter would result in a GFP-negative section in the mutant amnion that may or may not further transdifferentiate into the aggregate.

(**B-E**) Whole-mount pictures of chimeric embryos derived from GFP+ WT (B, E7.5) or *Smad5⁻ᐟ⁻* ESCs (C-E, left panels); and longitudinal sections of the same embryos stained with anti-GFP antibody (green). See also **Fig. S5**. Epiblast ectoderm inclusion (C-D) as well as ExEc inclusion (E, arrowhead) were observed. Amniotic aggregates (D, arrow) were always GFP+. Scale bars: whole mount: 100 μm, sections: 50 μm.
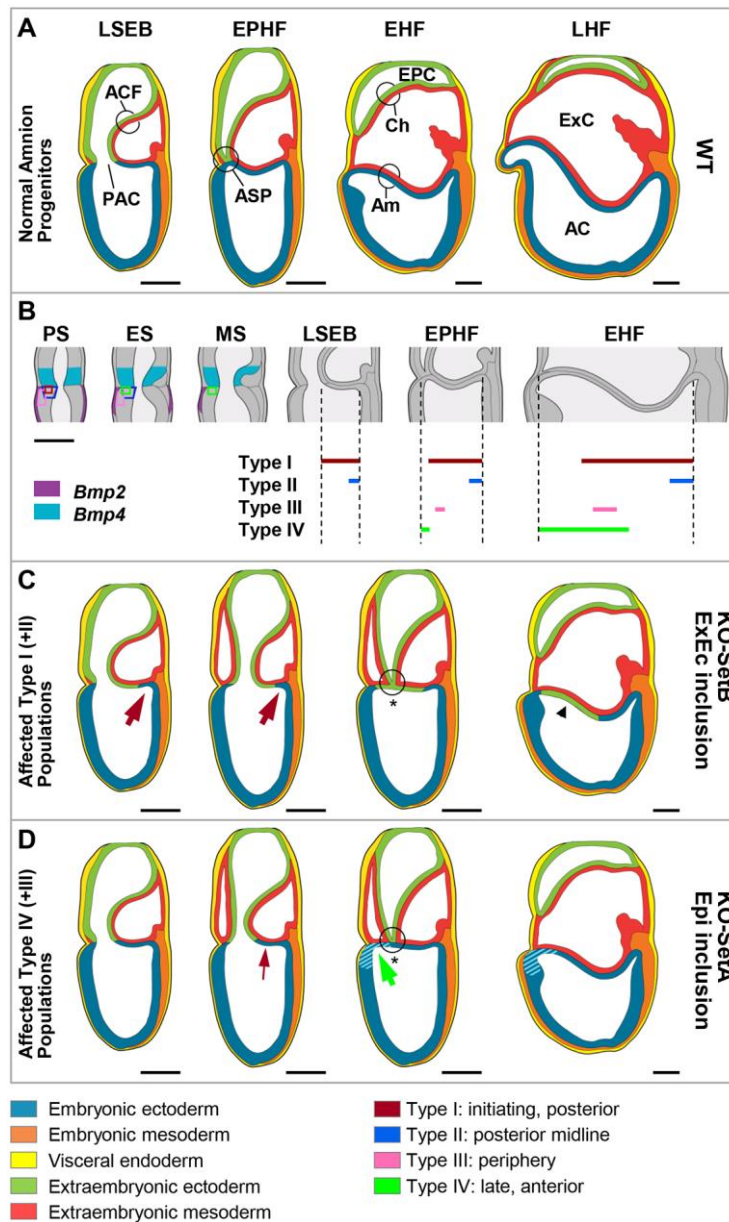
Figure 8. Model of normal and abnormal amniogenesis

(A) Schematic representation of normal amnion expansion.

(B) Expression of BMP ligands and spatio-temporal region of the progenitors of the different clone types contributing to amniotic ectoderm (regions in respective colour) at PS, ES and MS stages. *Bmp2* (Madabhushi and Lacy, 2011) and *Bmp4* (Lawson et al., 1999) are expressed in the 3 stages, the expression of *Bmp8b* (Ying and Zhao, 2001) in ExEc is only reported at ES (not drawn in scheme). Representation of amniotic contribution of descendants of the four different clone types (**Fig. 2, 3B**).

(C-D) Two sets of amnion defects occur in *Smad5* mutants. A posteriorized closure of the PAC and ASP (circle with asterisk) are in common, indicative of a deficit in Type I descendants (burgundy arrow).

(**C**) In few mutants (KO-SetB), a major deficiency in descendants of Type I and presumably also a reduction in the Type II amniotic ectoderm contribution cause an early posterior amniotic ectoderm deficit that may lead to cuboidal chorionic extraembryonic ectoderm trapping into the amniotic environment at PAC closure (arrowhead).

(**D**) In most mutants (KO-SetA), the population of Type IV (and III) is undersized (green arrow) with consequent inclusion of non-amniotic epiblast in amnion, or alternatively, anterior amniotic ectoderm differentiation stalls precluding the cuboidal-to-squamous transition of this epithelium (both represented by light-blue stripes). In these mutants, the atypical ectoderm will transdifferentiate in an amniotic aggregate with posterior streak mesoderm features.

Epiblast (D) and extraembryonic inclusion (C) defects may occur together, but our data are not conclusive on this point.

Scale bars: 100 μm. AC: amniotic cavity; ACF: amniochorionic fold; Am: amnion; ASP: anterior separation point; Ch: chorion; EHF: early headfold; EPC: ectoplacental cavity; EPHF: early preheadfold; ExC: exocoelomic cavity; LHF: late headfold; LSEB: late streak early allantoic bud; PAC: proamniotic canal.

Type	Clone	Colour-code/shape[1]	Initial stage[2]	Final stage[2]	Nominal age (E[3] days) at labelling	Clone age (hr)	Clone size	Cdt[4] (hr)	Amniotic Ectoderm	Amniotic Mesoderm	Posterior streak	Allantois	Yolk sac Mesoderm	PGC[5]	Surface ectoderm	Rest of embryo
Type I	1	Magenta/C	PS	LPHF/EHF	6.05	45	67	7.42	19 (28%)	0	8 (12%)	32 (48%)	0	3 (5%)	0	5[6] (7%)
	2	Dark blue/C	PS	EHF	6.19	41	31	8.28	23 (74%)	0	0	5 (16%)	0	0	0	3[6] (10%)
	3	[unplotted] [7]	PS+	3/4S	6.27	42.5	52	7.35	16 (31%)	0	12 (23%)	24 (46%)	0	0	0	0
Type II	4	Magenta/C	PS	EPHF	6.27	42.5	62	8.58 [2]	2 (3%)	0	8 (13%)	38 (63%)	3 (5%)	10 (16%)	0	0
	5	Dark blue/C	PS-	EPHF	6.21	42	69	6.9	9 (13%)	5 (7%)	0	45 (65%)	6 (9%)	0	0	4[6] (6%)
	6	Black/C	PS-	LSEB	6.12	44	84	6.88	2 (2%)	0	22[8] (26%)	30 (36%)	8 (10%)	4 (5%)	0	18[8,9] (21%)
	7	Green/C	PS-	LPHF	6.18	39	~150	~6.26 [2]	7 (4%)	1 (0.6%)	6 (4%)	26 (17%)	36 (23%)	0	18 (15%)	56[8,9] ((36%)
	8	Light green/C	PS-	LSEB	6.29	40.5	18	9.71	2 (11%)	0	6 (33%)	4 (23%)	0	6 (33%)	0	0
	9	Magenta/T	ES	4/5 S	6.69	40	43	7.37	15 (35%)	0	7 (16%)	21 (49%)	0	0	0	0
	10	Black/T	ES	6 S	6.64	40.5	40	7.61	3 (8%)	0	~30 (75%)	~7 (17%)	0	0	0	0
	11	Purple/T	ES	6 S	6.54	42	39	7.95	6 (15%)	0	0	0	33 (85%)	0	0	0
	12	Orange/T	ES-	5/6S	6.69	40	95	6.09	8 (8%)	0	9 (10%)	40 (42%)	38 (40%)	0	0	0
	13	Dark blue/T	ES+	EPHF/LPHF	6.55	19.75	11	5.71	4 (36%)	0	5 (46%)	0	2 (18%)	0	0	0
	14	Grey/T	ES	5S	6.59	41	~100	~7.26 [2]	2 (2%)	0	13 (13%)	85 (85%)	0	0	0	0
	15	Light green/T	ES	LPHF	6.71	22.5	18	5.4	2 (11%)	0	9 (50%)	7 (39%)	0	0	0	0
Type III	16	Magenta/C	PS	LSEB	6.65	24.5	35	5.93 [2]	5 (14%)	0	0	0	0	0	24 (69%)	6[10] (17%)
	17	Dark blue/T	ES+	3S	6.5	40	31	8.07	8 (26%)	0	0	0	0	0	23 (74%)	0
	18	Black/T	ES-	(L)PHF	6.85	21	10	6.32	2 (20%)	0	0	0	0	0	8 (80%)	0
	19	Grey/T	ES+	6/7S	6.88	37.5	27	7.89	5 (19%)	0	0	0	0	0	22[11] (81%)	0
	20	Green/C	PS/ES-	7S	6.57	41.5	73	6.7	10 (14%)	0	0	6 (8%)	0	0	57 (78%)	0
	21	Light green/T	ES	6S	6.48	42.75	~250	~6.14 [2]	14 (6%)	0	~27 (11%)	12 (5%)	0	0	~197 (78%)	0
	22	Orange/C	PS	LHF	6.67	40.5	44	7.42	8 (20%)	0	0	9 (20%)	0	0	27 (60%)	0
Type IV	23	Magenta/T	ES+	EHF	6.57	24.5	16	6.06	16 (100%)	0	0	0	0	0	0	0
	24	Dark blue/S	MS-	LPHF	6.67	20.25	14	5.32	14 (100%)	0	0	0	0	0	0	0
	25	Grey/S	MS	LHF	6.54	19.25	22	5.56 [2]	22 (100%)	0	0	0	0	0	0	0
	26	Green/T	ES+	5S	6.84	36	16	9	16 (100%)	0	0	0	0	0	0	0
	27	Light green/S	MS	LPHF	6.57	23	14	6.04	14 (100%)	0	0	0	0	0	0	0
Type IV + II	28	Black/T	ES-	3S	6.59	41	90	6.32	38 (42%)	0	10 (11%)	42 (47%)	0	0	0	0

Table 1. Record of clones contributing to amniotic ectoderm (see also **Table S5**)

(1)Used in Fig. 2, C: circle, S: square; T: triangle; (2)Stage terminology as in (Lawson and Wilson 2016); (3)E: embryonic day (see Materials and Methods for details); (4)Clone doubling time (Cdt) extracted from Fig. S1. [2] refers to 2 sibling progenitors: this affects the calculation of the Cdt; (5) PGC contribution of clones 1, 3, 5 and 7 was summarized in (Lawson and Hage 1994); (6)Proximal mesoderm; (7) Insufficient spatial detail recorded for plotting; (8)Posterior half of the streak; (9)Lateral plate mesoderm; (10)Distal half of the epiblast; (11) 3 Buccal, 2 oral plate, 11 VEAP (Cajal et al., 2012), 2 surface ectoderm at MB/HB, 4 surface ectoderm at S4.

Stage	ExEc Inclusion	Epiblast Inclusion without Aggregate				Epiblast Inclusion with Aggregate				Other[1]	Total
		Head-out & Thick AmEc	Thick AmEc	Head-out	Total Epiblast Inclusion	Anterior	Midline	Posterior	Total Aggregate		
E7.5-E8.0	3	7	9	-	16	-	-	-	-	2	21
E8.5 >4S	-	1	-	4	5	1	2	3	6	3	14
Total	3(9%)	8	9	4	21(60%)	1	2	3	6 (17%)	5(14%)	35

Table 2. Mutant chimeric phenotypes resulting from tetraploid complementation assay with *Smad5* KO GFP+ ESCs.

[1]Other: two chimeras without visible amnion; two chimeras with control phenotype; one very small embryo.

ExEc: extraembryonic ectoderm; AmEc: amniotic ectoderm.

B (continued)

E6.19 E6.47 E6.74 E7.02 E7.30 E7.58 E7.86 E8.13 E8.41

Clone 7
Initial age, E days 6.18
Final age, E days 7.805
Clone age, hrs 39
Clone size ~150
Cdt, hrs ~6.26 (2)

Generation (k)	0	1	2	3	4	5	6	Found 6.23
Embryo age, days	6.18	6.44	6.7	6.96	7.22	7.49	7.75	7.81
Cells	2	4	8	16	32	64	128	~150

Clone 8
Initial age, E days 6.29
Final age, E days 7.98
Clone age, hrs 40.5
Clone size 18
Cdt, hrs 9.71 (6.8 for non PGC, 16 for PGC)

solution a
solution b

Generation (k)	0	1	2	3	4	5	6	Found 4.17
Embryo age, days	6.29	6.57	6.86	7.14	7.42	7.71	7.99	7.98
Cells	1	2	4	8	16	32	64	18

Clone 9
Initial age, E days 6.69
Final age, E days 8.357
Clone age, hrs 40
Clone size 15
Cdt, hrs 7.37

Generation (k)	0	1	2	3	4	5	Found 5.43
Embryo age, days	6.69	7.00	7.30 7.45 7.61	7.92	8.23	8.36
Cells	1	2	4	8	16	32	43

Clone 10
Initial age, E days 6.64
Final age, E days 8.328
Clone age, hrs 40.5
Clone size 40
Cdt, hrs 7.61

Generation (k)	0	1	2	3	4	5	Found 5.32
Embryo age, days	6.64	6.96	7.27	7.59	7.91 8.07	8.23	8.33
Cells	1	2	4	8	16	32	40

Clone 11
Initial age, E days 6.54
Final age, E days 8.29
Clone age, hrs 42
Clone size 39
Cdt, hrs 7.95

Generation (k)	0	1	2	3	4	5	Found 5.29
Embryo age, days	6.54	6.87	7.20	7.53 7.70 7.86		8.20	8.29
Cells	1	2	4	8	16	32	39

Clone 12
Initial age, E days 6.69
Final age, E days 8.357
Clone age, hrs 40
Clone size 95
Cdt, hrs 6.09

Generation (k)	0	1	2	3	4	5	6	Found 6.57
Embryo age, days	6.69	6.94	7.20	7.45 7.58 7.70	7.96		8.21	8.36
Cells	1	2	4	8	16	32	64	95

Clone 13
Initial age, E days 6.55
Final age, E days 7.37
Clone age, hrs 19.75
Clone size 11
Cdt, hrs 5.71

Generation (k)	0	1	2	3	Found 3.46
Embryo age, days	6.55	6.79	7.03 7.15 7.26	7.37
Cells	1	2	4	8	11

B (continued)

Column time points: E6.19 · E6.47 · E6.74 · E7.02 · E7.30 · E7.58 · E7.86 · E8.13 · E8.41

Clone 14
Initial age, E days 6.59
Final age, E days 8.298
Clone age, hrs 41
Clone size ~100
Cdt, hrs 7.26 (2)

	Generation (k)	0	1	2	3	4	5	Found 5.64
	Embryo age, days	6.59	6.89	7.20	7.50	7.8	8.10	8.30
	Cells	2	4	8	16	32	64	~100

epiblast/streak: 2, 4, 8, 16
amniotic ectoderm: 1, 2, 2
posterior streak: 3, 6, 5, 10, 13
allantois: 13, 26, 52, 85

Clone 15
Initial age, E days 6.71
Final age, E days 7.648
Clone age, hrs 22.5
Clone size 18
Cdt, hrs 5.4

	Generation (k)	0	1	2	3			Found 4.17
	Embryo age, days	6.71	6.94	7.16	7.39	7.50	7.61	7.65
	Cells	1	2	4	8		16	18

epiblast: 1, 2, 4, 8
amniotic ectoderm: 1, 2, 2
surface ectoderm: 4, 8, 9
allantois: 3, 6, 7

C

Type III

Clone 16
Initial age, E days 6.65
Final age, E days 7.67
Clone age, hrs 24.5
Clone size 35
Cdt, hrs 5.93 (2)

	Generation (k)	0	1	2	3	4	Found 4.13
	Embryo age, days	6.65	6.90	7.14	7.39	7.63	7.67
	Cells	2	4	8	16	32	35

epiblast: 2, 4, 8
surface ectoderm: 7, 14
amniotic ectoderm: 1+1, 2+2, 4
(amniotic ectoderm): 12, 24, 1
surface ectoderm: 23
distal half embr. ectoderm: 1, 2, 4, 6

Clone 17
Initial age, E days 6.5
Final age, E days 8.167
Clone age, hrs 40
Clone size 31
Cdt, hrs 8.07

	Generation (k)	0	1	2		3	4	Found 4.95
	Embryo age, days	6.5	6.84	7.17	7.34	7.51	7.84	8.17
	Cells	1	2	4		8	16	31

epiblast: 1, 2, 4
amniotic ectoderm: 1, 2, 4, 8
surface ectoderm: 3, 6, 12, 23

Clone 18
Initial age, E days 6.85
Final age, E days 7.725
Clone age, hrs 21
Clone size 10
Cdt, hrs 6.32

	Generation (k)	0	1	2		3	Found 3.32
	Embryo age, days	6.85	7.11	7.38	7.51	7.64	7.73
	Cells	1	2	4		8	10

epiblast: 1, 2, 4
amniotic ectoderm: 1, 2, 2
surface ectoderm: 3, 6, 8

Clone 19
Initial age, E days 6.88
Final age, E days 8.443
Clone age, hrs 37.5
Clone size 27
Cdt, hrs 7.89

	Generation (k)	0	1	2		3	4	Found 4.75
	Embryo age, days	6.88	7.21	7.54	7.70	7.87	8.12	8.44
	Cells	1	2	4		8	16	27

epiblast: 1, 2, 4
amniotic ectoderm: 1, 2, 4, 5
surface ectoderm: 3, 6, 12, 22

Clone 20
Initial age, E days 6.57
Final age, E days 8.299
Clone age, hrs 41.5
Clone size 73
Cdt, hrs 6.7

	Generation (k)	0	1	2	3		4	5	6	Found 6.19
	Embryo age, days	6.57	6.85	7.13	7.41	7.55	7.69	7.97	8.24	8.30
	Cells	1	2	4	8		16	32	64	73

epiblast: 1, 2, 4, 8
amniotic ectoderm: 1, 2, 4, 8, 10
surface ectoderm: 7, 14, 13, 26, 52, 57
epiblast/streak: 1, 2
allantois: 4, 6

Clone 21
Initial age, E days 6.48
Final age, E days 8.26
Clone age, hrs 42.75
Clone size ~250
Cdt, hrs 6.14 (2)

	Generation (k)	0	1	2	3	4	5	6	Found 6.95
	Embryo age, days	6.48	6.74	6.99	7.25	7.50	7.76	8.02	8.26
	Cells	2	4	8	16	32	64	128	~250

epiblast: 2, 4, 8, 16
amniotic ectoderm: 1, 2, 4, 8, 14
surface ectoderm: 15, 30, 25, 50, 100, ~197
epiblast/streak: 5, 10, 7, 14, ~27
allantois: 3, 6, 12

Clone 22
Initial age, E days 6.67
Final age, E days 8.358
Clone age, hrs 40.5
Clone size 44
Cdt, hrs 7.42

	Generation (k)	0	1	2		3	4	5	Found 5.46
	Embryo age, days	6.67	6.98	7.29	7.44	7.60	7.91	8.22	8.36
	Cells	1	2	4		8	16	32	44

epiblast: 1, 2, 4
amniotic ectoderm: 1, 2, 4, 8, 8
surface ectoderm: 2, 4, 8, 16, 27
epiblast/streak: 1, 2
allantois: 4, 8, 9

Legend
- epiblast
- epiblast/streak
- streak
- amniotic ectoderm
- posterior streak
- allantois
- surface ectoderm
- distal half embr. ectoderm

D

| | E6.19 | E6.47 | E6.74 | E7.02 | E7.30 | E7.58 | E7.86 | E8.13 | E8.41 |

Type IV + Type II

| Clone | 28 | Generation (k) | 0 | 1 | 2 | 3 | 4 | 5 | 6 | Found 6.49 |

| Initial age, E days | 6.59 | Embryo age, days | 6.59 | 6.85 | 7.12 | 7.25 | 7.38 | 7.51 | 7.64 | 7.91 | 8.17 | 8.30 |

Final age, E days	8.3	Cells	1	2	4	8	16	32	64	90
Clone age, hrs	41
Clone size	90
Cdt, hrs	6.32

Diagram rows (cells):
- epiblast: 1, 2, 4
- amniotic ectoderm: 1, 2, 4, 8, 16, 28
- epiblast/streak: 3, 6; amniotic ectoderm: 1, 2, 4, 8, 10
- posterior streak: 1, 2, 4, 8, 10
- allantois: 4, 8, 16, 32, 42

Legend:
- epiblast
- epiblast/streak
- streak
- amniotic ectoderm
- posterior streak
- allantois

Figure S1. Inferred clonal histories of clones contributing to amniotic ectoderm.
Histories of: (**A**) Type I, (**B**) Type II, (**C**) Type III and (**D**) Type IV + Type II are shown.

1. Exponential growth is assumed. Then $N = a.e^{bt}$, or $\ln N_t = \ln N_0 + bt$, where N_t is final clone size, N_0 is initial clone size (usually 1, but 2 when siblings still joined by a cytoplasmic bridge were labelled), t is clone age. Clone doubling time (Cdt) is $\ln 2 / b = \ln 2 \times t / \ln N_t - \ln N_0$. The number of cell generations (k) is derived from $2^k = N_t / N_0$, then $k = \ln N_t - \ln N_0 / \ln 2$.
2. When estimating the distribution of cell generations, the first generation is expected to be shortened because the likelihood of impaling a columnar cell associated with the basement membrane and near the middle of the cell cycle is greater than impaling a mitotic or early post-mitotic one at the lumen (Gardner and Cockroft, 1998). When 2 siblings are initially labelled, the first generation is assumed to require a whole cell cycle.
3. No evidence for any significant difference in cell cycle length within the epiblast in the proximal half of the egg cylinder or its descendants between E6 and E8 has been found (Lawson et al., 1991; Tzouanacou et al., 2009) except for the PGCs. The contribution to PGCs in clones 1, 4, 6 and 8 was calculated according to (Lawson and Hage, 1994), modified to accommodate cell cycle lengthening during specification (McLaren and Lawson, 2005) until the PGC founding population closed at allocation (*).
4. In mixed clones, the calculated generation of entry into the amniotic ectoderm is supported by the 'found' distribution of the rest of the clone, although the intermediate distribution of the latter will be speculative if intermediate generations have transited through the streak, and possibly other regions. In contrast, the time of transition of pure clones from the epiblast to the amniotic ectoderm cannot be formally obtained: therefore no clonal histories are provided for Type IV clones that contributed exclusively to amniotic ectoderm.
5. Clonal data: The distribution of descendants 'found' is shown in the last column of Table 1 with its 8 subcolumns ("Clone distribution"). Differences from the calculated distribution at the last whole generation include natural variation (e.g. loss of cell cycle synchrony, apoptosis) and counting errors, as well as the difference between the final age of the clone and the calculated number of completed generations. Separation to a new cell category is made in the earliest possible cell generation, but does not exclude separation being made later by descendants. The estimate of the age at which the first cell in the amniotic ectoderm would have divided is used for comparison within and between clone types (see main text). Clone 8 has two possible solutions: one cell death (†) is assumed in order to account for the low number of somatic cells found (12) compared with expected (16 in solution a, 32 or 40 in solution b). E days (top row, in red) are a guide for the rough alignment of the clonal histories: they are based on the Cdts of the displayed clones with a start time from the E6.2 group.
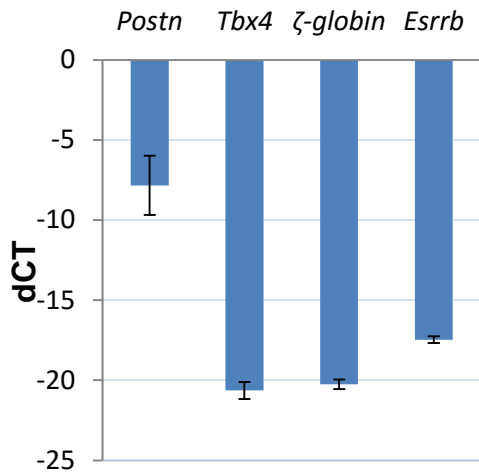
Figure S2. Possible explanation for the absence of Type I clones of amniotic ectoderm after injection at ES.

The cellular conformation at the embryonic-extraembryonic interface differs between PS (A) and ES (B) stages of development. At the ES stage (B), junctional anterolateral epiblast cells appear compressed and the interface tilts proximally towards the proamniotic cavity. The extraembryonic ectoderm is painted green. Images of frontal slices through embryo reconstructions reproduced from e-MouseAtlas (http://www.emouseatlas.org/emap/ema/home/.php) (Armit et al., 2017). A: EMA:8: TS8 (frontal:: pitch 90, yaw 257, roll 90, d 0), B: EMA:9: TS9 (frontal: pitch 94, yaw 69, roll 90, d -16).
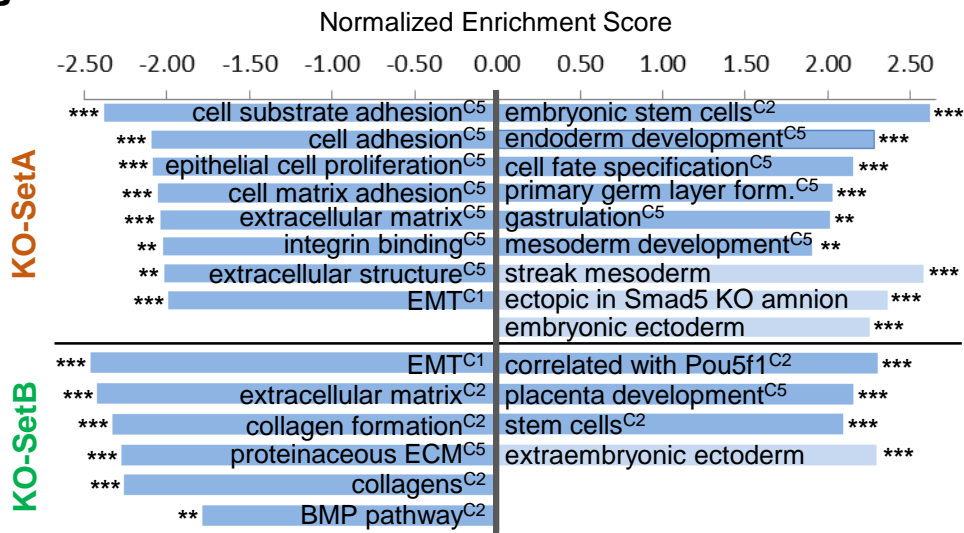
Either conformational difference would reduce the chance of successfully injecting an epiblast cell at the interface. This could account for the seven non-amniotic clones in the, apparently extreme proximal, anterolateral region (Fig.1, right panel): those progenitors may have been less close to the interface than they appeared.

An additional reason for the absence of type I clones at ES stage is that four labelled descendants from the PS stage could become available to join the amniochorionic fold at MS/LS compared with only two from the ES stage.
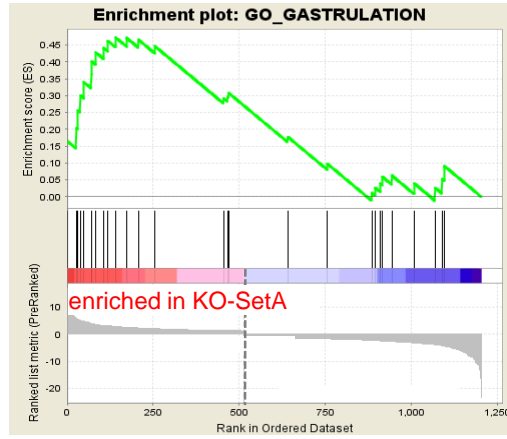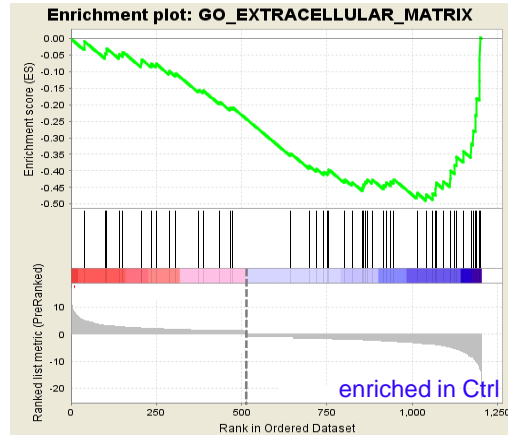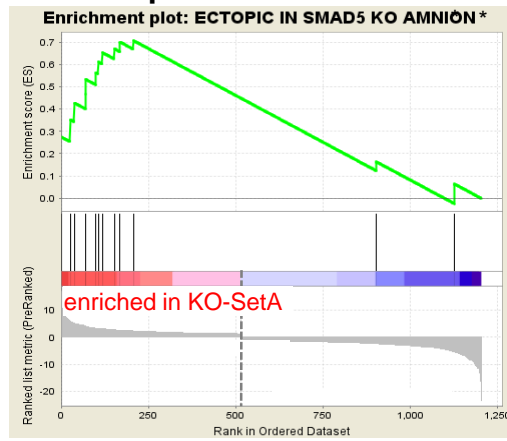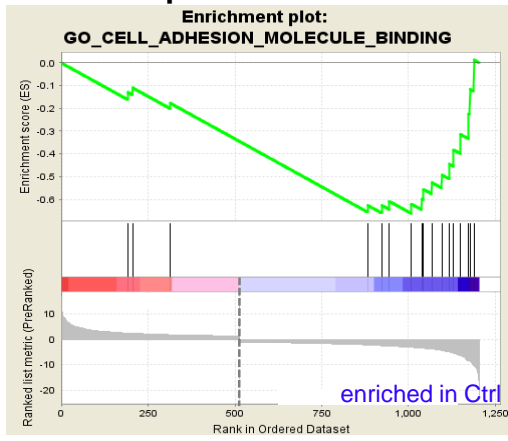
A

B

C **UNDER-expressed**   **OVER-expressed**

Figure S3. Analysis of differentially expressed genes shows two sets of mutants with distinct signatures

(**A**) qPCR validation of microdissected amniotic tissue. Amniotic cDNA obtained after microdissection is free from contamination with surrounding tissues, as shown by qPCR analysis for the six control amnion samples for: *Postn*, amnion marker; *Tbx4*, allantois marker; *ζ-globin*, visceral yolk sac marker; and *Esrrb*, chorion marker. KO samples were not included in the analysis due to the unknown origin of the amniotic aggregate and its streak features. For each gene, *Psmd4* normalized ΔCt values as means of the six replicates is represented, together with standard deviation (error bars).

(**B-C**) Gene set enrichment analysis (GSEAPreranked). The algorithm inquires whether a set of related genes (e.g. Gene Ontology (GO) terms) is enriched in the top or the bottom of a ranked list of transcripts (i.e. enriched in KO or Ctrl, see Supplemental Materials and Methods).

(**B**) A summary of selected gene sets sorted by Normalized Enrichment Score. Statistical significances: nominal p-value: ***: $p<0.001$, **: $p<0.01$, *: $p<0.05$.
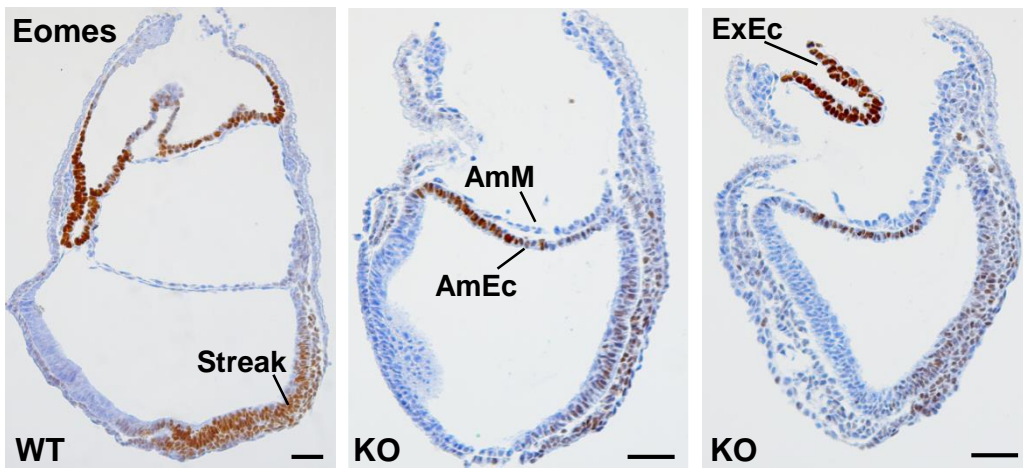
Dark blue bars: gene sets from the Molecular Signature Database (Libertzon et al., 2011) from categories C1, C2 and C5 (see Supplemental Materials and Methods).

Light blue bars: custom-made gene sets (see Table S3). "Ectopic in Smad5 KO amnion" comprises previously reported ectopically expressed genes in the mutant amnion/aggregate (Bosman et al., 2006; Pereira et al., 2012; unpublished data).
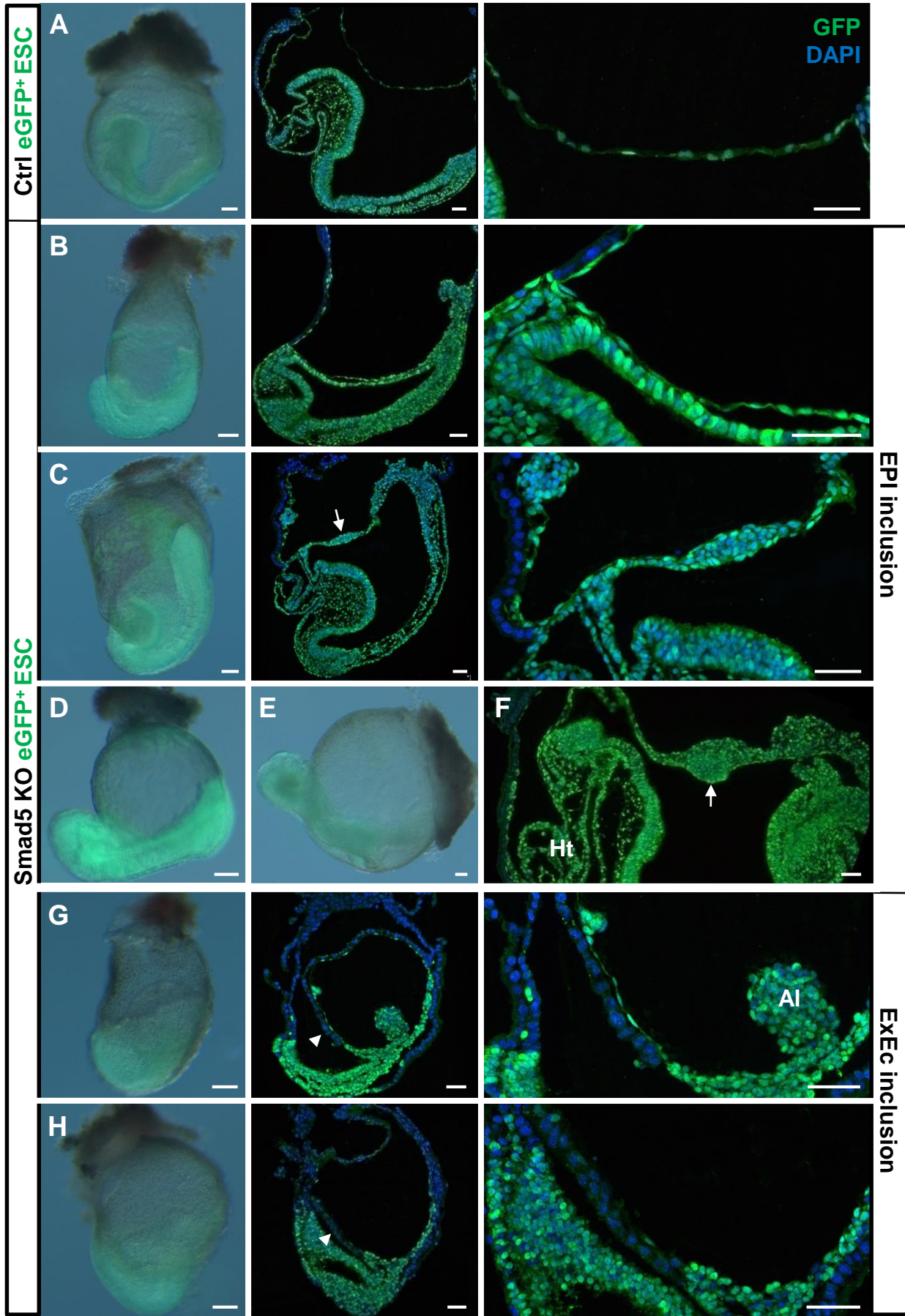
EC - extracellular. Gene set official names, searchable on http://software.broadinstitute.org/gsea/msigdb/genesets.jsp: Enriched in KO-SetA vs Ctrl: BENPORATH_ES_1, GO_ENDODERM_DEVELOPMENT, GO_CELL_FATE_SPECIFICATION, GO_CELL_FATE_COMMITMENT_INVOLVED_IN_FORMATION_OF_PRIMARY_GERM_LAYER, GO_GASTRULATION, GO_MESODERM_DEVELOPMENT. Enriched in Ctrl vs. KO-SetA: GO_REGULATION_OF_CELL_SUBSTRATE_ADHESION, GO_POSITIVE_REGULATION_OF_CELL_ADHESION, GO_REGULATION_OF_EPITHELIAL_CELL_PROLIFERATION, GO_REGULATION_OF_CELL_MATRIX_ADHESION, GO_EXTRACELLULAR_MATRIX, GO_INTEGRIN_BINDING, GO_EXTRACELLULAR_STRUCTURE_ORGANIZATION, HALLMARK_EPITHELIAL_MESENCHYMAL_TRANSITION. Enriched in KO-SetB vs. Ctrl: KORKOLA_CORRELATED_WITH_POU5F1, GO_PLACENTA_DEVELOPMENT, CONRAD_STEM_CELL. Enriched in Ctrl vs. KO-SetB: HALLMARK_EPITHELIAL_MESENCHYMAL_TRANSITION, REACTOME_EXTRACELLULAR_MATRIX_ORGANIZATION, REACTOME_COLLAGEN_FORMATION, GO_PROTEINACEOUS_EXTRACELLULAR_MATRIX, NABA_COLLAGENS, PID_BMP_PATHWAY.

(**C**) Selected GSEAPreranked enrichment plots are shown as examples for under- and over-represented gene sets, for the comparisons KO-SetA vs. Ctrl and KO-SetB vs. Ctrl. Custom-made gene sets are marked with an asterisk, see also Table S2. The green line in the graph represents the enrichment profile, and the vertical lines are individual hits; ES – (not normalized) Enrichment Score.

Figure S4. **Localization of Eomes protein at E7.5.** Immunohistochemistry on longitudinal sections of *Smad5* KO and littermate WT embryos. Eomes was detected in the streak and ExEc of both KO and WT. In KO, Eomes is also present in the amniotic ectoderm (AmEc) which is negative in the WT. The KO panels are serial sections of the same embryo. AmM – amniotic mesoderm. Scale bar: 50 µm.

Figure S5. Amnion paucity can be compensated by different inclusion mechanisms.
Whole-mount pictures of chimeric embryos derived from GFP+ WT (**A**, E8.5) or Smad5 KO
ES cells (**B-E, G-H**, left panels); and longitudinal sections of the same embryos stained with
anti-GFP antibody. Epiblast ectoderm (EPI) inclusion (**B-C**), as well as ExEc inclusion (**G-H**,
arrowhead) were observed. Amniotic aggregates (**C**, **F**, arrows) were always GFP+ indicating
their ESC/epiblast origin. Of note, some control and knockout chimeras had scattered
mosaic epiblast derived tissues (Figs 7, S4, data not shown), which confirmed the
observation that about half of the tetraploid acceptor embryos in a complementation setting
are competent for the epiblast lineage as well (Eakin et al., 2005; Wen et al., 2014). E8.5
chimeras with extreme head-out phenotype are shown in **D** and **E**. Ht – heart; Al – allantois.
Scale bars: whole mount: 100 µm, sections: 50 µm.

Figure S6. Proliferation and apoptosis seem unaffected in mutant amniotic ectoderm, but cell morphology and matrix proteins are disturbed in anterior amniotic ectoderm. (**A**) TUNEL assay and anti-pH3 staining in E7.0 control (n=10) and knockout (n=11) embryos before amnion-chorion separation. Negligible levels of apoptosis were detected in the amniochorionic fold (ACF). Scale bar: 50 μm.
(**B**) The average number of proliferating cells in the ectodermal component of the ACF in the same control and knockout embryos did not show significant difference (Mann-Whitney U test, p=0.69).

Figure S7. Antibody staining against ColIV and Postn.
Longitudinal sections of (**A**) E7.5 and (**B**) E8.5 Ctrl and Smad5 KO embryos stained agaist ColIV. In Ctrl, ColIV is distributed uniformly in the ECM between both amniotic ectoderm (AmEc) and amniotic mesoderm (AmM) cells. In knockouts, ColIV showed control-like distribution in regions of smooth amnion. In contrast, ColIV was not found between the ectodermal cells in the regions with thickened AmEc. Nuclei were stained with DAPI. Boxed area is magnified. The asterisks marks a sectioning artefact in the amnion. Scale bar: 100 µm, magnifications: 25 µm. (**C**) Localization of the amnion marker Postn (red) at E8.5. Postn is absent from the aggregate in mutants, while it is uniformly present in Ctrl amnion and in the bilayered portion of KO amnion. Nuclei are stained with DAPI (blue). Boxed area is magnified. Scale bar: 100 µm, magnifications: 25 µm.

Sample: name	type	Dev. stage	Sex	cDNA (ng)	Quality Score[1]	Input reads	% Mapping reads	Uniquely mapping reads	% Uniquely Mapped reads	% Assigned reads[2]
1.1	Ctrl	3S	♂	2175	22.96	61606749	37.8%	16394731	26.61%	88.48%
1.2	KO (SetA)	2S	♂	792	22.66	38123491	36.3%	8506141	22.31%	90.03%
2.1	Ctrl	LHF	♀	2025	22.98	49977574	38.9%	13664269	27.34%	89.21%
2.2	KO (SetB)	LHF	♀	3900	22.96	35827685	37.5%	8160168	22.78%	89.59%
3.1	Ctrl	EHF	♀	3240	22.94	44399436	37.0%	11957350	26.93%	88.10%
3.2	KO (SetA)	EHF	♀	3420	23.32	37937138	38.7%	10396617	27.40%	86.01%
4.1	Ctrl	EHF	♂	9750	23.22	33135579	38.3%	8504605	25.67%	88.77%
4.2	KO (SetB)	EHF	♀	3480	22.5	27438303	34.9%	5583741	20.35%	91.51%
5.1	Ctrl	LHF	♂	3240	23.2	40918085	38.4%	10183882	24.89%	90.07%
5.2	KO (SetB)	LPHF	♀	3690	22.7	58659608	36.3%	13600007	23.18%	90.21%
6.1	Ctrl[3]	EPHF	♂	3900	23.26	34087196	38.9%	9083874	26.65%	87.24%
6.2	KO (SetA)	EPHF	♂	3600	22.86	36364341	38.3%	9523991	26.19%	87.28%

Table S1. RNA-Seq sample details and alignment statistics.
The KO and Ctrl sample of each pair (e.g., 1.1 and 1.2) are obtained from littermates.
[1]Mean Quality Scores of the SOLiD reads per sample according to the Solexa scale (highest=40, lowest=15).
[2]uniquely mapped reads overlapping known annotated features (i.e. transcripts and exons).
[3]Sample 6.1 was initially genotyped as a control sample; however it appeared more similar to the KO samples in RNA-seq. It was excluded from further analysis.
S – somites; LHF – late headfold; EHF – early headfold; LPHF – late pre-headfold; EPHF). – early pre-headfold.
KO-SetB samples are in green, KO-SetA in orange. SetA and SetB are the categories attributed later to these samples (see text).

EMBRYONIC ECTODERM	***Fgf5, Gbx2, Fgf8, Zic3, Zic5, Six2, Zic2, Sox3, Tcfap2c, Tcfap2a,*** *Sox1, Nes, Msx2,* *Dlx5, Dlx3, Msx1, Trp63, Krt8, Krt15, Eya1, Six4, Sox2, Otx2, Six3, Hesx1, Sox1, Irx3, Foxg1, Six3, Otx2, Wnt1, Emx2, Pax6, Wnt8b, Pou3f1, Pax6, Map2, Zic1, Zic4, Sox2, Sox19, Hes1, Foxd4, Vax1, Irx2, Nkx1-2, Foxo1*
EXTRAEMBRYONIC ECTODERM	***Elf5, Cldn3, Esrrb, Sox21, Eomes, Cldn4, Sox2, Pcsk6,*** *Cited1, Bmp4, Hand1, Tcfap2a,* *Cdx2, Fgfr2, Ets2, Fgf8, Troma1, Gata3, Pl1, Pl2, Furin,*
STREAK MESODERM	***Eomes****, Fst, **T**, **Fgf8**, **Zic3**, **Mesp1**, **Mixl1**, **Tbx6**, **Lefty2**, **Mesp2**, **Wnt8a**, **Evx1**,* *Wnt3, Tdgf1, Cdx1, Epha2, Pdgfra, Hand1,* *Ecsit, Ext2, Hand2, Tlx2, Ext1, Foxf1a, Irx3, Lhx2, Srf, Kdr, Gsc, Lhx1, Fzd10, Hoxb1, Hoxb4, Hoxb8, Hoxa10, Cdx4, Foxh1, Foxa2, Foxc1, Foxc2, Hnf1a, Wnt3a, Wnt5a, Meox1, Lrp6, Srf, Fgf4, Fgf8, Vg1, Mixl1, Nog, Chrd, Tcf15, Pax1, Osr1, Twist1*
ECTOPIC IN SMAD5 KO AMNION	***Eomes, T, Fgf8, Mesp1, Mixl1, Lefty2, Nodal, Pou5f1, Wnt8a, Evx1, Wnt3,*** *Msx2, Fut4,* *Wnt3a, Ifitm2, Ifitm3, Alpl, Hba-x, Notch1, Gata4, Tbx2, Gsc, Foxa2, Meox1, Tcf15, Lhx1, Kdr*

Table S2. Lists of genes in each GSEA custom gene set shown in Fig. S2B. The genes enriched (core enrichment) in the top or bottom of the ranked lists of genes with cut-off p-adj. <0.05 are in bold. The genes not in bold are not enriched, and the genes in grey are not found in the ranked lists. The gene set "Ectopic in Smad5 KO amnion" contains genes previously found to be ectopically expressed in Smad5 KO amnion at mRNA or protein level (Chang et al., 1999; Bosman et al., 2006; Pereira et al., 2012; unpublished data).

	UNDER-expressed	OVER-expressed
KO-SetA vs. Ctrl		
Markers for primitive streak and streak-derived mesoderm		*Nodal, Tdgf1, Fgf8, Eomes, T, Fst, Wnt8a, Mesp1, Mesp2, Evx1, Mixl1, Tbx6*
EMT related genes		*Mmp9, Wnt3, Wnt5b*
BMP target genes and modulators	*Postn, Hand1, Hey2, Id4, Flrt3, Smoc2*	*Zic2, Zic3, Zic5*
Nodal and Nodal target genes		*Nodal, Eomes, Tdgf1 (Cripto), Lefty2, Wnt3, Fgf5, Mesp1, Mixl1*
Stem cell and PGC markers		*Pou5f1 (Oct4), Nanog, Fgf4, Tfap2c, Prdm1 (Blimp1), Prdm14*
Genes rich in amnion	*Postn, Flrt3*	
Collagens and integrins	*Col5a2, Col9a1, Col1a1, Col1a2, Col12a1, Itga4, Itga8*	
KO-SetB vs. Ctrl		
Extraembryonic ectoderm markers		*Eomes, Esrrb, Sox2, Elf5, Cldn3, Cldn4, Pcsk6, Ets2, Cited1, Sox21, Sox15*
BMP signaling components, target genes and modulators	*Bmp2, Bmp4, Smoc2, Nog, Gata4, Gata5, Gata6, Msx1, Msx2, Hand1, Hand2, Hes1, Id3, Id4, Tgfb2, Tgfbr1, Tgfbr3, Vegfa, Vegfc, Dlx2, Dlx5, Smad6, Smad1, Smad9, Smad2, Smad7, Hey2, Twist1, Twist2, Acvr1, Mmp2, Postn, Flrt3, Bmp2k, Mef2a, Cited2*	*Bmp8a, Bmp8b, Id2, Cited1, Zic5*
Genes rich in amnion	*Tfap2a,Twist1,Flrt3*	
Pluripotency-associated markers		*Dppa2, Dppa4*
Collagens and integrins	*Col9a1, Col4a5, Col5a2, Col5a1, Col1a1, Col1a2, Col4a2, Col4a1, Col4a3bp, Col23a1, Col3a1, Col4a6, Col27a1, Col26a1, Col8a2, Itga8, Itgb1*	

Table S3. Differential expression analysis highlights (cut-off: padj. <0.05).

A

Gene ID	Gene Name	Ctrl 1.1	Ctrl 2.1	Ctrl 3.1	Ctrl 4.1	Ctrl 5.1	KO 1.2	KO 3.2	KO 6.2	KO 2.2	KO 4.2	KO 5.2
ENSMUSG00000029337	*Fgf5*	0.0463522	0.0463522	0.2781130	0.9270433	0.0463522	5.0987380	16.2232571	9.2240805	0.0463522	0.0463522	0.0463522
ENSMUSG00000037171	*Nodal*	0.2766748	0.0553350	0.0553350	0.0553350	0.0553350	3.6521080	2.9327534	3.6521080	0.0553350	1.2727043	0.0553350
ENSMUSG00000062327	*T*	36.756044	41.212840	20.981992	104.309046	12.519089	216.480080	1006.735027	279.426057	34.051921	38.909327	26.540468
ENSMUSG00000066652	*Lefty2*	0.9767862	0.0443994	0.0443994	2.3531667	0.7547893	24.3308558	12.3430254	2.3087673	1.2431824	0.4883931	0.0443994
ENSMUSG00000027186	*Elf5*	0.0591765	0.2564315	0.1972550	0.1972550	0.3156080	0.5128630	0.1183530	0.0591765	70.8145430	42.6465298	76.6335654
ENSMUSG00000021255	*Esrrb*	0.0958548	0.1533676	0.1533676	0.0191710	0.6134705	0.3450772	0.0958548	0.0191710	39.3963110	33.9709309	39.3963110
ENSMUSG00000047501	*Cldn4*	0.3191816	0.5106906	0.0638363	0.5745269	1.0213811	0.0638363	0.8937085	0.0638363	33.0033783	24.7684928	43.2810261
ENSMUSG00000074637	*Sox2*	3.6068608	6.5374352	4.0577184	6.8755784	1.5780016	3.2687176	18.9923764	3.8322896	92.9893799	35.2232500	56.0190567
					Ctrl			KO-SetA			KO-SetB	

B

Selected genes enriched in KO-SetA

Gene ID	Comparison	log$_2$ Fold Change	p.adj.
Fgf5	KO-setA vs Ctrl	6.16075779794208	1.81873385913884e-10
	KO-setB vs Ctrl	-1.74310062924334	0.331548627984435
	KO-SetB vs KO-SetA	-7.90385842718541	1.23115117082365e-08
Nodal	KO-setA vs Ctrl	4.59725897942216	0.000585195595286753
	KO-setB vs Ctrl	2.17085268679028	0.16287679917155
	KO-SetB vs KO-SetA	-2.42640629263189	0.150176193285943
T	KO-setA vs Ctrl	3.58132861465481	9.12924374983415e-07
	KO-setB vs Ctrl	-0.380749064181876	0.724006771706442
	KO-SetB vs KO-SetA	-3.96207767883669	1.00111017881162e-06
Lefty2	KO-setA vs Ctrl	4.51797067858599	0.000470896168512567
	KO-setB vs Ctrl	-0.418754191923372	0.834151087607506
	KO-SetB vs KO-SetA	-4.93672487050937	0.000734872133795889

Selected genes enriched in KO-SetB

Gene ID	Comparison	log$_2$ Fold Change	p.adj.
Elf5	KO-setA vs Ctrl	0.279899263412563	0.880161463820885
	KO-setB vs Ctrl	8.61394649337021	1.46436300266915e-34
	KO-SetB vs KO-SetA	8.33404722995764	8.15847149665294e-25
Esrrb	KO-setA vs Ctrl	-0.0178525607789109	0.992880455772707
	KO-setB vs Ctrl	7.65968085084086	3.64140098797345e-21
	KO-SetB vs KO-SetA	7.67753341161977	6.68665855440136e-16
Cldn4	KO-setA vs Ctrl	-0.446928095611415	0.819841766795906
	KO-setB vs Ctrl	6.0755960548316	2.80619696632073e-16
	KO-SetB vs KO-SetA	6.52252415044302	1.81992898403329e-12
Sox2	KO-setA vs Ctrl	1.03108493636301	0.359532368834508
	KO-setB vs Ctrl	3.92605097755526	5.49265480860401e-08
	KO-SetB vs KO-SetA	2.89496604119225	0.00136752480201529

Table S4. Comparative analysis of selected markers representative for KO-SetA and KO-SetB *Smad5* mutant amnion. (A) Normalized expression counts (FPKM) of individual RNA-Seq samples. (B) Comparison of differential expression of the selected markers between the three groups of replicates.

Clone	Embryo identity[1]	Mouse strain	Label	h, w (µm)[2]
1	039201	B6CBA[3]	LRDX	107,153
2	149103	B6CBA	LRDX	122,138
3	169204	B6CBA	LRDX	153,168
4	169205	B6CBA	LRDX	138,153
5	149211	B6CBA	LRDX	145,145
6	149201	B6CBA	LRDX	120,130
7	379107	B6CBA	LRDX	130,138
8	149217	B6CBA	LRDX	130,122
9	279216	B6CBA	LRDX	168,168
10	279211	B6CBA	LRDX	207,199
11	269205	B6CBA	LRDX	184,168
12	279215	B6CBA	LRDX	207,184
13	240104	B6CBA	HRP/LRDX	283,245
14	439005	B6CBA	LRDX	230,214
15	468506	Dub:ICR[4]	HRP/LRDX	na
16	518607	Dub:ICR	HRP/LRDX	209,221
17	359901	B6CBA	HRP/LRDX	260,230
18	528507	Dub:ICR	HRP/LRDX	na
19	128709	Dub:ICR	HRP/LRDX	353,379
20	269208	B6CBA	LRDX	184,199
21	269202	B6CBA	LRDX	230,199
22	409008	B6CBA	LRDX	122,153
23	280805	B6CBA	HRP/LRDX	214,191
24	190812	B6CBA	HRP/LRDX	184,230
25	410101	B6CBA	HRP/LRDX	367,283
26	828608	Dub:ICR	HRP/LRDX	412,279
27	190803	B6CBA	HRP/LRDX	237,199
28	269210	B6CBA	LRDX	230,161

Table S5. List of clones.
[1]The number is a unique embryo/clone identifier. [2]Height (h) and width (w) of the embryonic portion at dissection. [3]C57BL/6 x CBA.Ca or F1 matings. [4]Dub:ICR embryos are larger than BL6CBA, but less developmentally advanced, during E6 - E7.5.

Gene	Forward primer 5' – 3'	Reverse primer 5' – 3'
RT-qPCR		
Postn	AAGGAAAAGGGTCATACACGTACTTC	CCTCTGCGAATGTCAGAATCC
Tbx4	TCAACACCTTCCCAACTCAG	GGGAGAACGGAAATAGTGATCG
ζ-globin	GCTTCAAGATCATGACCGCCGT	CGGTGGAGGCTTAGCGGTACTT
Esrrb	CCATGCACAAACTCTTCCTG	CACTTGGATCGTGTCCGTC
Gapdh	AAGAAGGTGGTGAAGCAGGC	GCCTCTCTTGCTCAGTGTCC
Psmd4	GTTCCTTCAGAGCGTCCTAG	CTATCCAACCCCGTCTTTACAG
Nodal	AAAAGTGTTGGCATCAGCCC	TGGTGCTGGCGACAGGTAC
Lefty2	TCCTTGCCCATGATTGTCAG	CTGACGAGAGCACTAAGTTAGG
T	AACAGCTCTCCAACCTATGC	TACCATTGCTCACAGACCAG
Elf5	CCGAGTGGTTAAGTCAGAAGC	CGGTGTCCATCAGAGTTTCTC
Cldn4	CCGCCAGCAACTATGTGTAAG	ACGGGCTAGTAACTTTGCAC
Sox2	GATCAGCATGTACCTCCCC	CCCTCCCAATTCCCTTGTATC
Fgf5	ACTTTCCTTCACCGTCACTG	GTATCCGAGTTTCCTTCAGGG
Sex genotyping		
Jarid1cd	CTGAAGCTTTTGGCTTTGAG	CCACTGCCAAATTCTTTGG
Sry	TGGGACTGGTGACAATTGTC	GAGTACAGGTGTGCAGCTCT
IL3	GGGACTCCAAGCTTCAATCA	TGGAGGAGGAAGAAAAGCAA
In situ hybridization		
Fgf5	ATTAACCCTCACTAAAGGGAAAACTC CATGCAAGTGCCAAA	TAATACGACTCACTATAGGGTTCC ACACGTGTAGGCACAG

Table S6. Lists of primers for RT-qPCR and sex genotyping PCR.

Supplemental Material and Methods

Gene Set Enrichment Analyzis (GSEA).

To detect enriched functional gene sets, we ran GSEA (Subramanian et al., 2005) in PreRanked mode using the list of differentially expressed genes for each contrast (KO-SetA/Ctrl and KO-SetB/Ctrl) with padj. <0.05, ranked by the signed log of the adjusted p-value. The resulting ranked lists consisted of the genes with the "strongest" up-regulation in KO at the top of the list and the genes with the "strongest" down-regulation in KO at the bottom of the list, with the genes not changing among conditions in the middle. GSEA v.3.0 in PreRanked mode was run with the most recent version of Molecular Signatures Database (MSigDB)(Liberzon et al., 2011) – v.6.1 updated in October 2017, using the following collections of gene sets: Hallmark gene sets (Liberzon et al., 2016)(50 sets), C2 – Curated gene sets (4738 sets including Canonical pathways databases from BioCarta, KEGG and Reactome, and from expression signatures of genetic and chemical perturbations from biomedical literature), and C5 – 5917 Gene Ontology (GO) terms including all ontologies (molecular function, cellular component, and biological process)(Consortium, 2000). Gene size limits we set at 5 to 500. In addition, 4 custom made gene sets were used. Enrichment of each set of related genes in the top or bottom of the KO/ctrl ranked lists of genes was assessed by GSEA's normalized enrichment score (NES). The enrichment score reflects the degree to which a gene set is overrepresented at the top or bottom of a ranked list of genes. GSEA calculates the ES by walking down the ranked list of genes, increasing a running-sum statistic when a gene is in the gene set and decreasing it when it is not. The magnitude of the increment depends on the correlation of the gene with the phenotype. The ES is the maximum deviation from zero encountered in walking the list. A positive ES indicates gene set enrichment at the top of the ranked list; a negative ES indicates gene set enrichment at the bottom of the ranked list (Subramanian et al., 2005). The nominal p-value was used to estimate the statistical significance of the NES for each particular set.

References:

Consortium, T. G. O. (2000). Gene ontologie: Tool for the unification of biology. Nature Genetics **25**, 25–29.

Eakin, G. S., Hadjantonakis, A.-K., Papaioannou, V. E. and Behringer, **R. R.** (2005). Developmental potential and behavior of tetraploid cells in the mouse embryo. Developmental biology **288**, 150–9.

Gardner, R. L. and Cockroft, D. L. (1998). Complete dissipation of coherent clonal growth occurs before gastrulation in mouse epiblast. Development (Cambridge, England) **125**, 2397–2402.

Lawson, K. A. and Hage, W. J. (1994). Clonal analysis of the origin of primordial germ cells in the mouse. Ciba Foundation symposium **182**, 68-84-91.

Lawson, K. A., Meneses, J. J. and Pedersen, R. A. (1991). Clonal analysis of epiblast fate during germ layer formation in the mouse embryo. Development (Cambridge, England) **113**, 891–911.

McLaren, A. and Lawson, K.A. (2005). How is the mouse germ-cell lineage established? Differentiation **73,**435-7.

Liberzon, A., Subramanian, A., Pinchback, R., Thorvaldsdóttir, H., Tamayo, P. and Mesirov, J. P. (2011). Molecular signatures database (MSigDB) 3.0. Bioinformatics **27**, 1739–1740.

Liberzon, A., Birger, C., Ghandi, M., Jill, P., Tamayo, P., Jolla, L. and Jolla, L. (2016). Collection. **1**, 417–425.

Subramanian, A., Tamayo, P., Mootha, V. K., Mukherjee, S., Ebert, B. L., Gillette, M. A., Paulovich, A., Pomeroy, S. L., Golub, T. R., Lander, E. S., et al. (2005). Gene set enrichment analysis: a knowledge-based approach for interpreting genome-wide expression profiles. Proceedings of the National Academy of Sciences of the United States of America **102**, 15545–50.

Tzouanacou, E., Wegener, A., Wymeersch, F. J., Wilson, V. and Nicolas, J. F. (2009). Redefining the Progression of Lineage Segregations during Mammalian Embryogenesis by Clonal Analysis. Developmental Cell **17**, 365–376.

Wen, D., Saiz, N., Rosenwaks, Z., Hadjantonakis, A. K. and Rafii, S. (2014). Completely ES cell-derived mice produced by tetraploid complementation using inner cell mass (ICM) deficient blastocysts. PLoS ONE **9,** e94730.

Supplementary Excel File: Top 100 most differentially expressed genes in KO-SetA or KO-SetB versus Ctrl amnion samples (RNA-Seq).

Click here to Download Supplementary Excel File

B (continued)

E6.19   E6.47   E6.74   E7.02   E7.30   E7.58   E7.86   E8.13   E8.41

Clone 7
Initial age, E days 6.18
Final age, E days 7.805
Clone age, hrs 39
Clone size ~150
Cdt, hrs ~6.26 (2)

	E6.19	E6.47	E6.74	E7.02	E7.30	E7.58	E7.86	E8.13 Found 6.23
Generation (k)	0	1	2	3	4	5	6	
Embryo age, days	6.18	6.44	6.7	6.96	7.22	7.49	7.75	7.81
Cells	2	4	8	16	32	64	128	~150

Row values: 2 1 2 4 8 | 1 2 4 8 7 ; 3 6 1 2 4 6 ; 5 10 20 26 ; 4 8 16 32 31 36 ; 1 1 ; 1 2 4 1 2 4 8 16 18 ; 3 6 12 24 48 56

Clone 8
Initial age, E days 6.29
Final age, E days 7.98
Clone age, hrs 40.5
Clone size 18
Cdt, hrs 9.71
(6.8 for non PGC, 16 for PGC)

								Found 4.17
Generation (k)	0	1	2	3	4	5	6	
Embryo age, days	6.29	6.57	6.86	7.14	7.42	7.71	7.99	7.98
Cells	1	2	4	8	16	32	64	18

solution a: 1 2 1 2 1 2 3+1† | 1 2 2 ; 1 2* 4 6 ; 2 4 3 6 6 ; 1 2 4 4

solution b: 1 1+1† 1 2 1 2 1 2 4 8 | 1 2 ; 1 2* 4 6 ; 4 6 ; 3 4

Clone 9
Initial age, E days 6.69
Final age, E days 8.357
Clone age, hrs 40
Clone size 15
Cdt, hrs 7.37

								Found 5.43
Generation (k)	0	1	2	3	4	5		
Embryo age, days	6.69	7.00	7.30 7.45	7.61	7.92	8.23	8.36	
Cells	1	2	4	8	16	32	43	

Row values: 1 2 4 | 1 2 4 8 15 ; 3 6 1 2 4 7 ; 5 10 20 21

Clone 10
Initial age, E days 6.64
Final age, E days 8.328
Clone age, hrs 40.5
Clone size 40
Cdt, hrs 7.61

								Found 5.32
Generation (k)	0	1	2	3	4	5		
Embryo age, days	6.64	6.96	7.27	7.59	7.91 8.07	8.23	8.33	
Cells	1	2	4	8	16	32	40	

Row values: 1 2 4 8 | 1 2 3 ; 16 12 24 ~30 ; 3 6 ~7

Clone 11
Initial age, E days 6.54
Final age, E days 8.29
Clone age, hrs 42
Clone size 39
Cdt, hrs 7.95

								Found 5.29
Generation (k)	0	1	2	3	4	5		
Embryo age, days	6.54	6.87	7.20	7.53 7.70	7.86	8.20	8.29	
Cells	1	2	4	8	16	32	39	

Row values: 1 2 4 8 | 1 2 4 6 ; 7 14 28 33

Clone 12
Initial age, E days 6.69
Final age, E days 8.357
Clone age, hrs 40
Clone size 95
Cdt, hrs 6.09

								Found 6.57
Generation (k)	0	1	2	3	4	5	6	
Embryo age, days	6.69	6.94	7.20	7.45 7.58	7.70	7.96	8.21	8.36
Cells	1	2	4	8	16	32	64	95

Row values: 1 2 4 8 | 1 2 4 8 8 ; 1 2 4 8 9 ; 3 6 12 24 40 ; 3 6 12 24 38

Clone 13
Initial age, E days 6.55
Final age, E days 7.37
Clone age, hrs 19.75
Clone size 11
Cdt, hrs 5.71

					Found 3.46
Generation (k)	0	1	2	3	
Embryo age, days	6.55	6.79	7.03 7.15	7.26	7.37
Cells	1	2	4	8	11

Row values: 1 2 4 | 1 2 4 ; 3 6 5 ; 2

B (continued)

	E6.19	E6.47	E6.74	E7.02	E7.30	E7.58	E7.86	E8.13	E8.41

Clone 14
Initial age, E days 6.59
Final age, E days 8.298
Clone age, hrs 41
Clone size ~100
Cdt, hrs 7.26 (2)

Generation (k): 0, 1, 2, 3, 4, 5, Found 5.64
Embryo age, days: 6.59, 6.89, 7.20, 7.50, 7.8, 8.10, 8.30
Cells: 2, 4, 8, 16, 32, 64, ~100

2	4	8	16		1	2	2
					3	6	5	10	13
					13	26		52	85

Clone 15
Initial age, E days 6.71
Final age, E days 7.648
Clone age, hrs 22.5
Clone size 18
Cdt, hrs 5.4

Generation (k): 0, 1, 2, 3, 4, Found 4.17
Embryo age, days: 6.71, 6.94, 7.16, 7.39, 7.50, 7.61, 7.65
Cells: 1, 2, 4, 8, 16, 18

1	2	4	8	1	2	2
				4	8	9
				3	6	7

C

	E6.19	E6.47	E6.74	E7.02	E7.30	E7.58	E7.86	E8.13	E8.41

Type III

Clone 16
Initial age, E days 6.65
Final age, E days 7 .67
Clone age, hrs 24.5
Clone size 35
Cdt, hrs 5.93 (2)

Generation (k): 0, 1, 2, 3, 4, Found 4.13
Embryo age, days: 6.65, 6.90, 7.14, 7.39, 7.63, 7.67
Cells: 2, 4, 8, 16, 32, 35

2	4	8	7	14	1+1	2+2	4
					12	24	1
							23
			1	2		4	6

Legend:
- epiblast
- epiblast/streak
- streak
- amniotic ectoderm
- posterior streak
- allantois
- surface ectoderm
- distal half embr. ectoderm

Clone 17
Initial age, E days 6.5
Final age, E days 8.167
Clone age, hrs 40
Clone size 31
Cdt, hrs 8.07

Generation (k): 0, 1, 2, 3, 4, Found 4.95
Embryo age, days: 6.5, 6.84, 7.17, 7.34, 7.51, 7.84, 8.17
Cells: 1, 2, 4, 8, 16, 31

| 1 | 2 | 4 | 1 | 2 | | 4 | | 8 |
| | | | 3 | 6 | | 12 | | 23 |

Clone 18
Initial age, E days 6.85
Final age, E days 7.725
Clone age, hrs 21
Clone size 10
Cdt, hrs 6.32

Generation (k): 0, 1, 2, 3, Found 3.32
Embryo age, days: 6.85, 7.11, 7.38, 7.51, 7.64, 7.73
Cells: 1, 2, 4, 8, 10

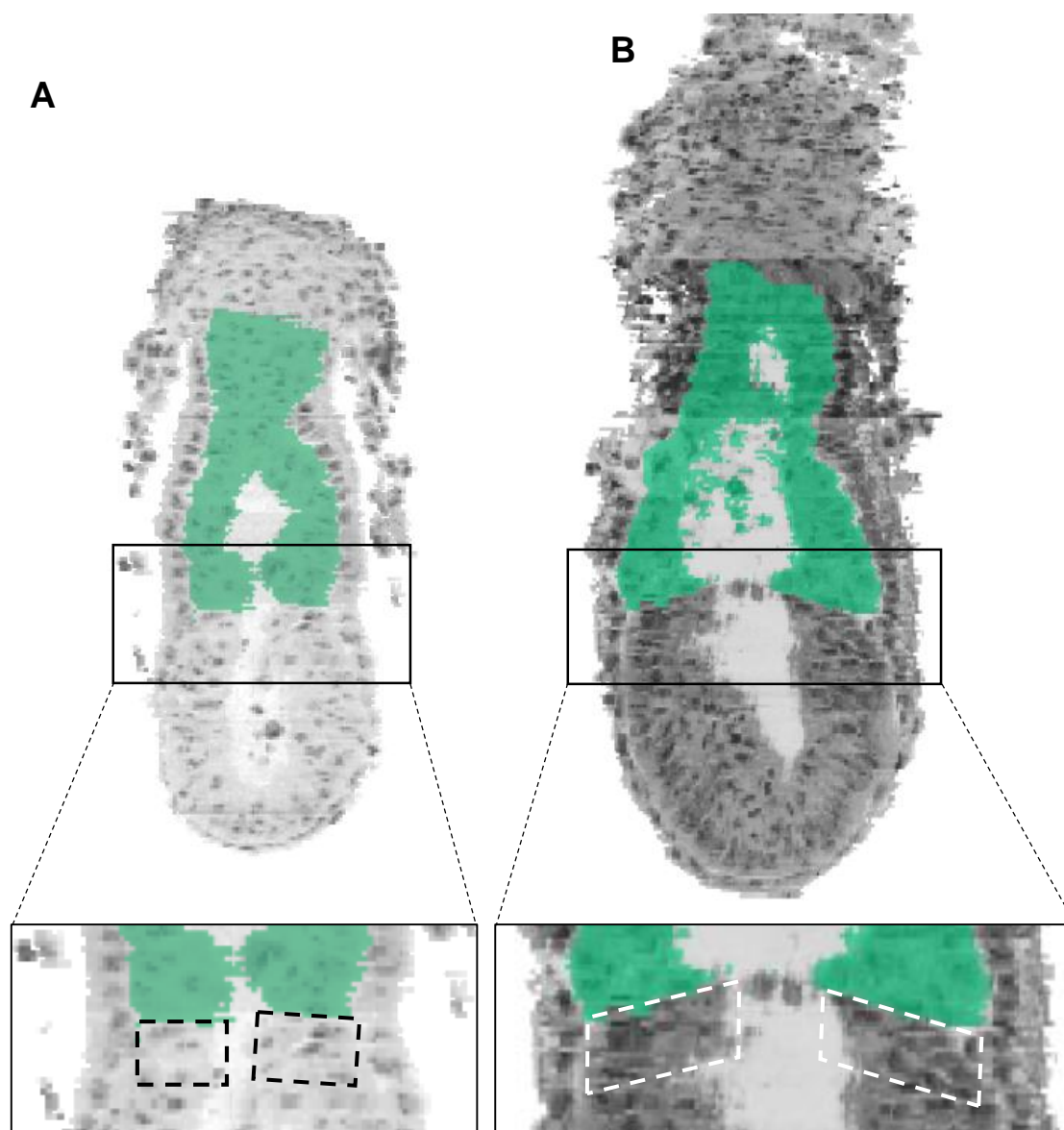| 1 | 2 | 4 | 1 | 2 | | 2 |
| | | | 3 | 6 | | 8 |

Clone 19
Initial age, E days 6.88
Final age, E days 8.443
Clone age, hrs 37.5
Clone size 27
Cdt, hrs 7.89

Generation (k): 0, 1, 2, 3, 4, Found 4.75
Embryo age, days: 6.88, 7.21, 7.54, 7.70, 7.87, 8.12, 8.44
Cells: 1, 2, 4, 8, 16, 27

| 1 | 2 | 4 | 1 | 2 | | 4 | | 5 |
| | | | 3 | 6 | | 12 | | 22 |

Clone 20
Initial age, E days 6.57
Final age, E days 8.299
Clone age, hrs 41.5
Clone size 73
Cdt, hrs 6.7

Generation (k): 0, 1, 2, 3, 4, 5, 6, Found 6.19
Embryo age, days: 6.57, 6.85, 7.13, 7.41, 7.55, 7.69, 7.97, 8.24, 8.30
Cells: 1, 2, 4, 8, 16, 32, 64, 73

1	2	4	8	1	2		4		8		10
				7	14	13	26		52		57
					1	2		4		6

Clone 21
Initial age, E days 6.48
Final age, E days 8.26
Clone age, hrs 42.75
Clone size ~250
Cdt, hrs 6.14 (2)

Generation (k): 0, 1, 2, 3, 4, 5, 6, Found 6.95
Embryo age, days: 6.48, 6.74, 6.99, 7.25, 7.50, 7.76, 8.02, 8.26
Cells: 2, 4, 8, 16, 32, 64, 128, ~250

2	4	8	16	1	2		4		8	14
				15	30	25	50		100	~197
					5	10	7	14	~27
						3	6	12

Clone 22
Initial age, E days 6.67
Final age, E days 8.358
Clone age, hrs 40.5
Clone size 44
Cdt, hrs 7.42

Generation (k): 0, 1, 2, 3, 4, 5, Found 5.46
Embryo age, days: 6.67, 6.98, 7.29, 7.44, 7.60, 7.91, 8.22, 8.36
Cells: 1, 2, 4, 8, 16, 32, 44

1	2	4	1	2		4		8		8
			2	4		8		16		27
			1	2		4		8		9

D

		E6.19	E6.47	E6.74	E7.02	E7.30	E7.58	E7.86	E8.13	E8.41

Type IV + Type II

| Clone 28 | Generation (k) | 0 | 1 | 2 | 3 | 4 | 5 | 6 | Found 6.49 |

| Initial age, E days 6.59 | Embryo age, days | 6.59 | 6.85 | 7.12 7.25 7.38 7.51 7.64 | 7.91 | 8.17 8.30 |

Final age, E days 8.3	Cells	1	2	4	8	16	32	64	90
Clone age, hrs 41									
Clone size 90									
Cdt, hrs 6.32									

Row data (colored bars):
- amniotic ectoderm: 1 2 4 | 1 2 4 8 16 28
- epiblast/streak → amniotic ectoderm: 3 6 1 2 4 8 10
- posterior streak: 1 2 4 8 10
- allantois: 4 8 16 32 42

Legend:
- epiblast
- epiblast/streak
- streak
- amniotic ectoderm
- posterior streak
- allantois

Figure S1. Inferred clonal histories of clones contributing to amniotic ectoderm.
Histories of: (**A**) Type I, (**B**) Type II, (**C**) Type III and (**D**) Type IV + Type II are shown.

1. Exponential growth is assumed. Then $N = a.e^{bt}$, or $\ln N_t = \ln N_0 + bt$, where N_t is final clone size, N_0 is initial clone size (usually 1, but 2 when siblings still joined by a cytoplasmic bridge were labelled), t is clone age. Clone doubling time (Cdt) is $\ln 2 / b = \ln 2 \times t / \ln N_t - \ln N_0$. The number of cell generations (k) is derived from $2^k = N_t / N_0$, then $k = \ln N_t - \ln N_0 / \ln 2$.

2. When estimating the distribution of cell generations, the first generation is expected to be shortened because the likelihood of impaling a columnar cell associated with the basement membrane and near the middle of the cell cycle is greater than impaling a mitotic or early post-mitotic one at the lumen (Gardner and Cockroft, 1998). When 2 siblings are initially labelled, the first generation is assumed to require a whole cell cycle.

3. No evidence for any significant difference in cell cycle length within the proximal half of the epiblast between E6 and E8 has been found (Lawson et al., 1991; Tzouanacou et al., 2009) except for the PGCs. The contribution to PGCs in clones 1, 4, 6 and 8 was calculated according to (Lawson and Hage, 1994), modified to accommodate cell cycle lengthening during specification (McLaren and Lawson, 2005) until the PGC founding population closed at allocation (*).

4. In mixed clones, the calculated generation of entry into the amniotic ectoderm is supported by the 'found' distribution of the rest of the clone, although the intermediate distribution of the latter will be speculative if intermediate generations have transited through the streak, and possibly other regions. In contrast, the time of transition of pure clones from the epiblast to the amniotic ectoderm cannot be formally obtained: therefore no clonal histories are provided for Type IV clones that contributed exclusively to amniotic ectoderm.

5. Clonal data: The distribution of descendants 'found' is shown in the last column of Table 1 with its 8 subcolumns ("Clone distribution"). Differences from the calculated distribution at the last whole generation include natural variation (e.g. loss of cell cycle synchrony, apoptosis) and counting errors, as well as the difference between the final age of the clone and the calculated number of completed generations. Separation to a new cell category is made in the earliest possible cell generation, but does not exclude separation being made later by descendants. The estimate of the age at which the first cell in the amniotic ectoderm would have divided is used for comparison within and between clone types (see main text). Clone 8 has two possible solutions: one cell death (†) is assumed in order to account for the low number of somatic cells found (12) compared with expected (16 in solution a, 32 or 40 in solution b). E days (top row, in red) are a guide for the rough alignment of the clonal histories: they are based on the Cdts of the displayed clones with a start time from the E6.2 group.
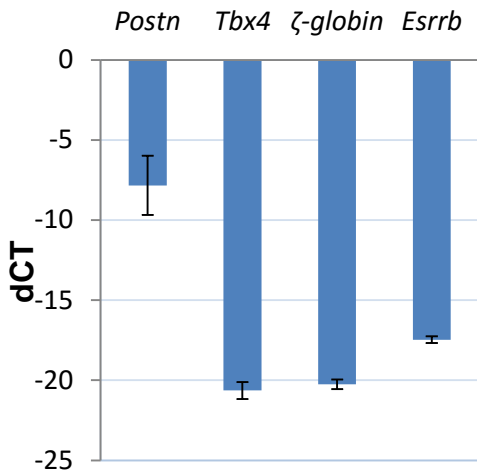
Figure S2. Possible explanation for the absence of Type I clones of amniotic ectoderm after injection at ES.
The cellular conformation at the embryonic-extraembryonic interface differs between PS (A) and ES (B) stages of development. At the ES stage (B), junctional anterolateral epiblast cells appear compressed and the interface tilts proximally towards the proamniotic cavity. The extraembryonic ectoderm is painted green. Images of frontal slices through embryo reconstructions reproduced from e-MouseAtlas (http://www.emouseatlas.org/emap/ema/home/.php) (Armit et al., 2017). A: EMA:8: TS8 (frontal:: pitch 90, yaw 257, roll 90, d 0), B: EMA:9: TS9 (frontal: pitch 94, yaw 69, roll 90, d -16).

Either conformational difference would reduce the chance of successfully injecting an epiblast cell at the interface. This could account for the seven non-amniotic clones in the, apparently extreme proximal, anterolateral region (Fig.1, right panel): those progenitors may have been less close to the interface than they appeared.

An additional reason for the absence of type I clones at ES stage is that four labelled descendants from the PS stage could become available to join the amniochorionic fold at MS/LS compared with only two from the ES stage.
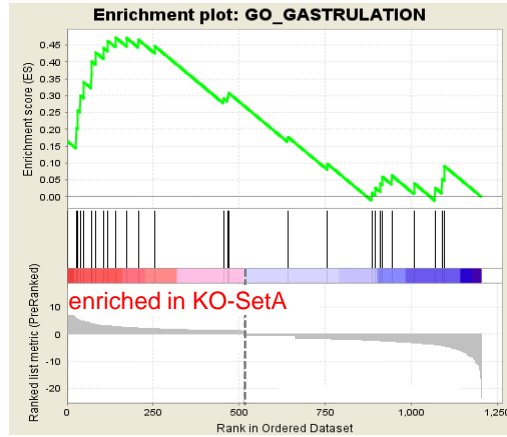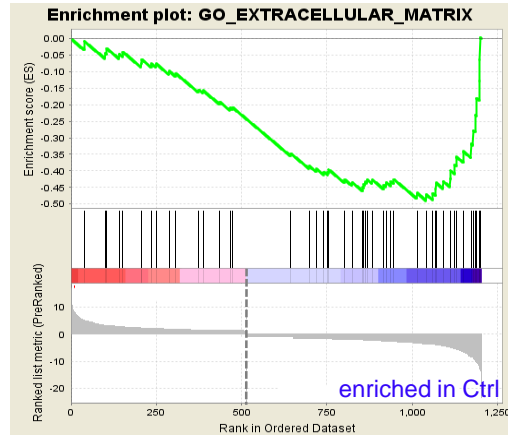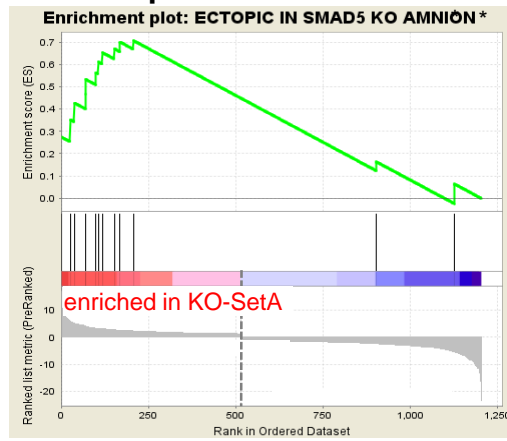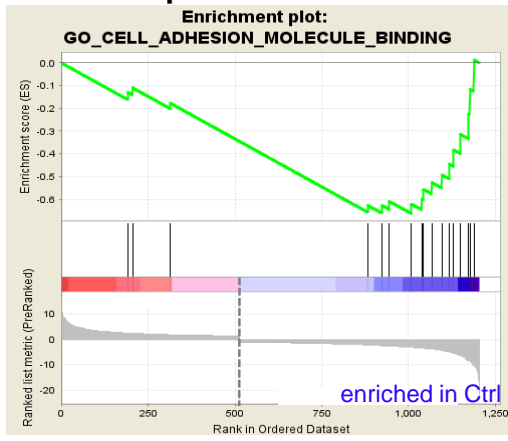
A

B

C **UNDER-expressed** **OVER-expressed**

Figure S3. Analysis of differentially expressed genes shows two sets of mutants with distinct signatures

(**A**) qPCR validation of microdissected amniotic tissue. Amniotic cDNA obtained after microdissection is free from contamination with surrounding tissues, as shown by qPCR analysis for the six control amnion samples for: *Postn*, amnion marker; *Tbx4*, allantois marker; *ζ-globin*, visceral yolk sac marker; and *Esrrb*, chorion marker. KO samples were not included in the analysis due to the unknown origin of the amniotic aggregate and its streak features. For each gene, *Psmd4* normalized ΔCt values as means of the six replicates is represented, together with standard deviation (error bars).

(**B-C**) Gene set enrichment analysis (GSEAPreranked). The algorithm inquires whether a set of related genes (e.g. Gene Ontology (GO) terms) is enriched in the top or the bottom of a ranked list of transcripts (i.e. enriched in KO or Ctrl, see Supplemental Materials and Methods).
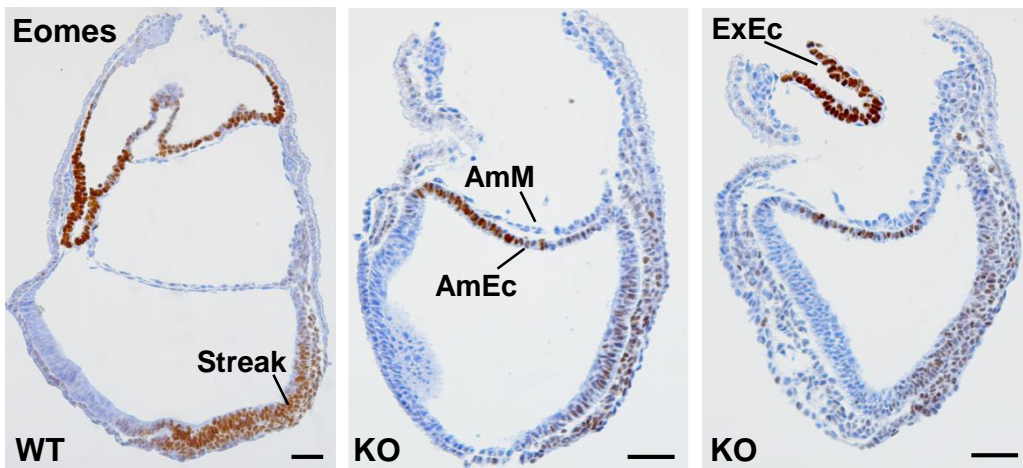
(**B**) A summary of selected gene sets sorted by Normalized Enrichment Score. Statistical significances: nominal p-value: ***: $p<0.001$, **: $p<0.01$, *: $p<0.05$.

Dark blue bars: gene sets from the Molecular Signature Database (Libertzon et al., 2011) from categories C1, C2 and C5 (see Supplemental Materials and Methods).
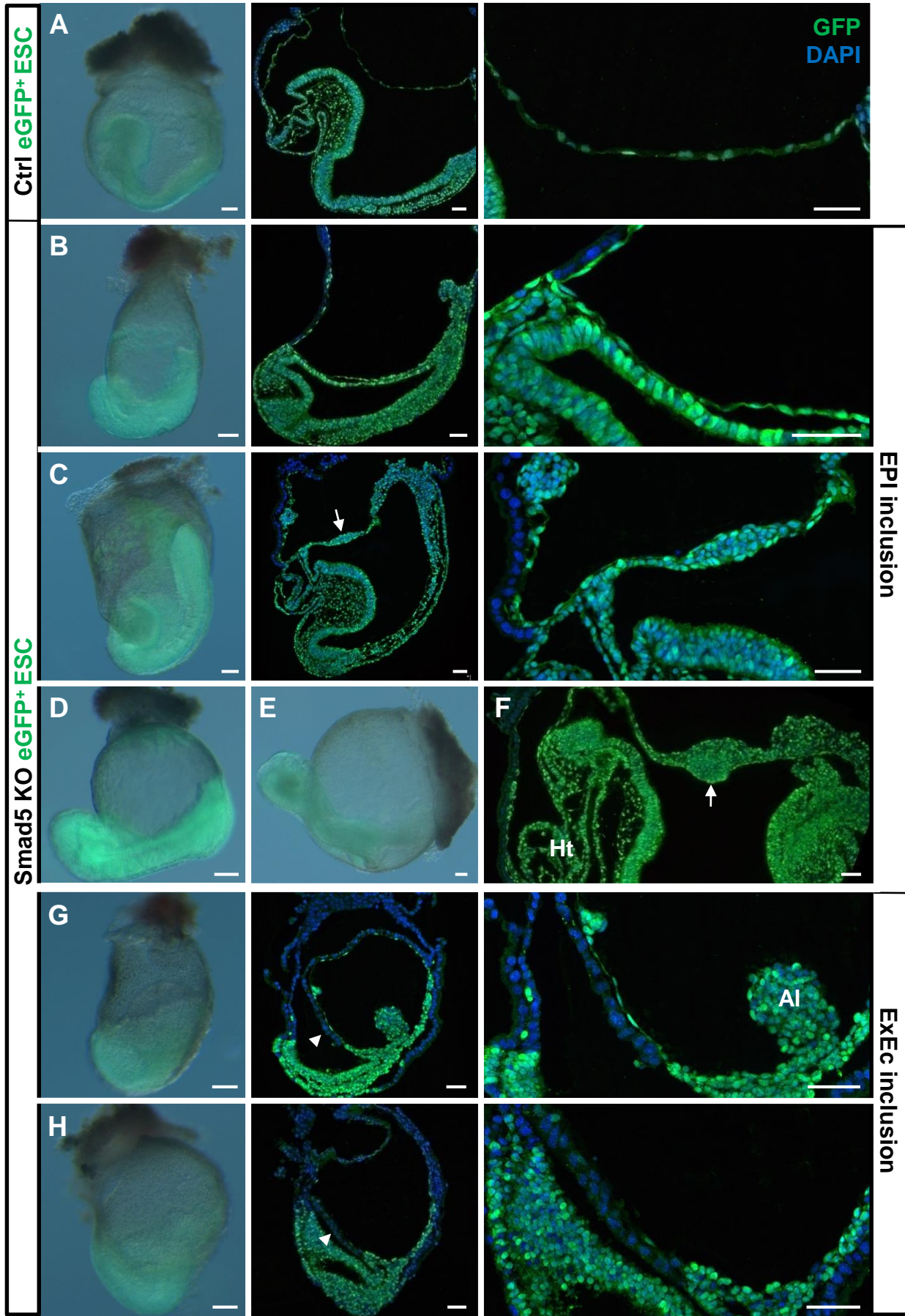
Light blue bars: custom-made gene sets (see Table S3). "Ectopic in Smad5 KO amnion" comprises previously reported ectopically expressed genes in the mutant amnion/aggregate (Bosman et al., 2006; Pereira et al., 2012; unpublished data).

EC - extracellular. Gene set official names, searchable on http://software.broadinstitute.org/gsea/msigdb/genesets.jsp: Enriched in KO-SetA vs Ctrl: BENPORATH_ES_1, GO_ENDODERM_DEVELOPMENT, GO_CELL_FATE_SPECIFICATION, GO_CELL_FATE_COMMITMENT_INVOLVED_IN_FORMATION_OF_PRIMARY_GERM_LAYER, GO_GASTRULATION, GO_MESODERM_DEVELOPMENT. Enriched in Ctrl vs. KO-SetA: GO_REGULATION_OF_CELL_SUBSTRATE_ADHESION, GO_POSITIVE_REGULATION_OF_CELL_ADHESION, GO_REGULATION_OF_EPITHELIAL_CELL_PROLIFERATION, GO_REGULATION_OF_CELL_MATRIX_ADHESION, GO_EXTRACELLULAR_MATRIX, GO_INTEGRIN_BINDING, GO_EXTRACELLULAR_STRUCTURE_ORGANIZATION, HALLMARK_EPITHELIAL_MESENCHYMAL_TRANSITION. Enriched in KO-SetB vs. Ctrl: KORKOLA_CORRELATED_WITH_POU5F1, GO_PLACENTA_DEVELOPMENT, CONRAD_STEM_CELL. Enriched in Ctrl vs. KO-SetB: HALLMARK_EPITHELIAL_MESENCHYMAL_TRANSITION, REACTOME_EXTRACELLULAR_MATRIX_ORGANIZATION, REACTOME_COLLAGEN_FORMATION, GO_PROTEINACEOUS_EXTRACELLULAR_MATRIX, NABA_COLLAGENS, PID_BMP_PATHWAY.

(**C**) Selected GSEAPreranked enrichment plots are shown as examples for under- and over-represented gene sets, for the comparisons KO-SetA vs. Ctrl and KO-SetB vs. Ctrl. Custom-made gene sets are marked with an asterisk, see also Table S2. The green line in the graph represents the enrichment profile, and the vertical lines are individual hits; ES – (not normalized) Enrichment Score.
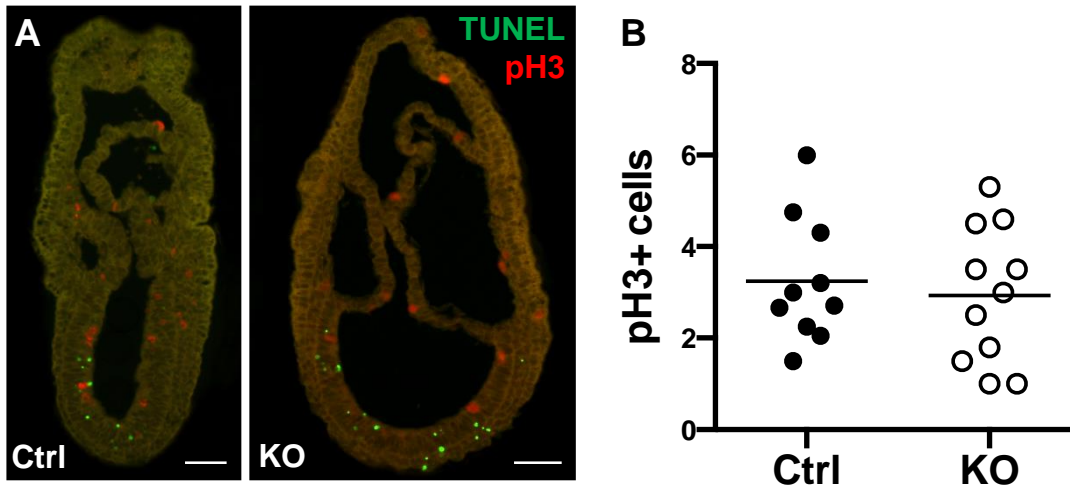
Figure S4. **Localization of Eomes protein at E7.5.** Immunohistochemistry on longitudinal sections of *Smad5* KO and littermate WT embryos. Eomes was detected in the streak and ExEc of both KO and WT. In KO, Eomes is also present in the amniotic ectoderm (AmEc) which is negative in the WT. The KO panels are serial sections of the same embryo. AmM – amniotic mesoderm. Scale bar: 50 µm.

Figure S5. Amnion paucity can be compensated by different inclusion mechanisms.
Whole-mount pictures of chimeric embryos derived from GFP+ WT (**A**, E8.5) or Smad5 KO ES cells (**B-E, G-H**, left panels); and longitudinal sections of the same embryos stained with anti-GFP antibody. Epiblast ectoderm (EPI) inclusion (**B-C**), as well as ExEc inclusion (**G-H**, arrowhead) were observed. Amniotic aggregates (**C**, **F**, arrows) were always GFP+ indicating their ESC/epiblast origin. Of note, some control and knockout chimeras had scattered mosaic epiblast derived tissues (Figs 7, S4, data not shown), which confirmed the observation that about half of the tetraploid acceptor embryos in a complementation setting are competent for the epiblast lineage as well (Eakin et al., 2005; Wen et al., 2014). E8.5 chimeras with extreme head-out phenotype are shown in **D** and **E**. Ht – heart; Al – allantois. Scale bars: whole mount: 100 µm, sections: 50 µm.

Figure S6. Proliferation and apoptosis seem unaffected in mutant amniotic ectoderm, but cell morphology and matrix proteins are disturbed in anterior amniotic ectoderm. (**A**) TUNEL assay and anti-pH3 staining in E7.0 control (n=10) and knockout (n=11) embryos before amnion-chorion separation. Negligible levels of apoptosis were detected in the amniochorionic fold (ACF). Scale bar: 50 µm.

(**B**) The average number of proliferating cells in the ectodermal component of the ACF in the same control and knockout embryos did not show significant difference (Mann-Whitney U test, p=0.69).

Figure S7. Antibody staining against ColIV and Postn.

Longitudinal sections of (**A**) E7.5 and (**B**) E8.5 Ctrl and Smad5 KO embryos stained agaist ColIV. In Ctrl, ColIV is distributed uniformly in the ECM between both amniotic ectoderm (AmEc) and amniotic mesoderm (AmM) cells. In knockouts, ColIV showed control-like distribution in regions of smooth amnion. In contrast, ColIV was not found between the ectodermal cells in the regions with thickened AmEc. Nuclei were stained with DAPI. Boxed area is magnified. The asterisks marks a sectioning artefact in the amnion. Scale bar: 100 μm, magnifications: 25 μm. (**C**) Localization of the amnion marker Postn (red) at E8.5. Postn is absent from the aggregate in mutants, while it is uniformly present in Ctrl amnion and in the bilayered portion of KO amnion. Nuclei are stained with DAPI (blue). Boxed area is magnified. Scale bar: 100 μm, magnifications: 25 μm.

Sample: name	Sample: type	Dev. stage	Sex	cDNA (ng)	Quality Score[1]	Input reads	% Mapping reads	Uniquely mapping reads	% Uniquely Mapped reads	% Assigned reads[2]
1.1	Ctrl	3S	♂	2175	22.96	61606749	37.8%	16394731	26.61%	88.48%
1.2	KO (SetA)	2S	♂	792	22.66	38123491	36.3%	8506141	22.31%	90.03%
2.1	Ctrl	LHF	♀	2025	22.98	49977574	38.9%	13664269	27.34%	89.21%
2.2	KO (SetB)	LHF	♀	3900	22.96	35827685	37.5%	8160168	22.78%	89.59%
3.1	Ctrl	EHF	♀	3240	22.94	44399436	37.0%	11957350	26.93%	88.10%
3.2	KO (SetA)	EHF	♀	3420	23.32	37937138	38.7%	10396617	27.40%	86.01%
4.1	Ctrl	EHF	♂	9750	23.22	33135579	38.3%	8504605	25.67%	88.77%
4.2	KO (SetB)	EHF	♀	3480	22.5	27438303	34.9%	5583741	20.35%	91.51%
5.1	Ctrl	LHF	♂	3240	23.2	40918085	38.4%	10183882	24.89%	90.07%
5.2	KO (SetB)	LPHF	♀	3690	22.7	58659608	36.3%	13600007	23.18%	90.21%
6.1	Ctrl[3]	EPHF	♂	3900	23.26	34087196	38.9%	9083874	26.65%	87.24%
6.2	KO (SetA)	EPHF	♂	3600	22.86	36364341	38.3%	9523991	26.19%	87.28%

Table S1. RNA-Seq sample details and alignment statistics.
The KO and Ctrl sample of each pair (e.g., 1.1 and 1.2) are obtained from littermates.
[1]Mean Quality Scores of the SOLiD reads per sample according to the Solexa scale (highest=40, lowest=15).
[2]uniquely mapped reads overlapping known annotated features (i.e. transcripts and exons).
[3]Sample 6.1 was initially genotyped as a control sample; however it appeared more similar to the KO samples in RNA-seq. It was excluded from further analysis.
S – somites; LHF – late headfold; EHF – early headfold; LPHF – late pre-headfold; EPHF). – early pre-headfold.
KO-SetB samples are in green, KO-SetA in orange. SetA and SetB are the categories attributed later to these samples (see text).

EMBRYONIC ECTODERM	***Fgf5, Gbx2, Fgf8, Zic3, Zic5, Six2, Zic2, Sox3, Tcfap2c, Tcfap2a,*** *Sox1, Nes, Msx2, Dlx5, Dlx3, Msx1, Trp63, Krt8, Krt15, Eya1, Six4, Sox2, Otx2, Six3, Hesx1, Sox1, Irx3, Foxg1, Six3, Otx2, Wnt1, Emx2, Pax6, Wnt8b, Pou3f1, Pax6, Map2, Zic1, Zic4, Sox2, Sox19, Hes1, Foxd4, Vax1, Irx2, Nkx1-2, Foxo1*
EXTRAEMBRYONIC ECTODERM	***Elf5, Cldn3, Esrrb, Sox21, Eomes, Cldn4, Sox2, Pcsk6,*** *Cited1, Bmp4, Hand1, Tcfap2a, Cdx2, Fgfr2, Ets2, Fgf8, Troma1, Gata3, Pl1, Pl2, Furin,*
STREAK MESODERM	***Eomes,*** *Fst,* ***T,*** *Fgf8,* ***Zic3, Mesp1, Mixl1, Tbx6, Lefty2, Mesp2, Wnt8a, Evx1,*** *Wnt3, Tdgf1, Cdx1, Epha2, Pdgfra, Hand1, Ecsit, Ext2, Hand2, Tlx2, Ext1, Foxf1a, Irx3, Lhx2, Srf, Kdr, Gsc, Lhx1, Fzd10, Hoxb1, Hoxb4, Hoxb8, Hoxa10, Cdx4, Foxh1, Foxa2, Foxc1, Foxc2, Hnf1a, Wnt3a, Wnt5a, Meox1, Lrp6, Srf, Fgf4, Fgf8, Vg1, Mixl1, Nog, Chrd, Tcf15, Pax1, Osr1, Twist1*
ECTOPIC IN SMAD5 KO AMNION	***Eomes, T, Fgf8, Mesp1, Mixl1, Lefty2, Nodal, Pou5f1, Wnt8a, Evx1, Wnt3,*** *Msx2, Fut4, Wnt3a, Ifitm2, Ifitm3, Alpl, Hba-x, Notch1, Gata4, Tbx2, Gsc, Foxa2, Meox1, Tcf15, Lhx1, Kdr*

Table S2. Lists of genes in each GSEA custom gene set shown in Fig. S2B. The genes enriched (core enrichment) in the top or bottom of the ranked lists of genes with cut-off p-adj. <0.05 are in bold. The genes not in bold are not enriched, and the genes in grey are not found in the ranked lists. The gene set "Ectopic in Smad5 KO amnion" contains genes previously found to be ectopically expressed in Smad5 KO amnion at mRNA or protein level (Chang et al., 1999; Bosman et al., 2006; Pereira et al., 2012; unpublished data).

	UNDER-expressed	**OVER-expressed**
KO-SetA vs. Ctrl		
Markers for primitive streak and streak-derived mesoderm		*Nodal, Tdgf1, Fgf8, Eomes, T, Fst, Wnt8a, Mesp1, Mesp2, Evx1, Mixl1, Tbx6*
EMT related genes		*Mmp9, Wnt3, Wnt5b*
BMP target genes and modulators	*Postn, Hand1, Hey2, Id4, Flrt3, Smoc2*	*Zic2, Zic3, Zic5*
Nodal and Nodal target genes		*Nodal, Eomes, Tdgf1 (Cripto), Lefty2, Wnt3, Fgf5, Mesp1, Mixl1*
Stem cell and PGC markers		*Pou5f1 (Oct4), Nanog, Fgf4, Tfap2c, Prdm1 (Blimp1), Prdm14*
Genes rich in amnion	*Postn, Flrt3*	
Collagens and integrins	*Col5a2, Col9a1, Col1a1, Col1a2, Col12a1, Itga4, Itga8*	
KO-SetB vs. Ctrl		
Extraembryonic ectoderm markers		*Eomes, Esrrb, Sox2, Elf5, Cldn3, Cldn4, Pcsk6, Ets2, Cited1, Sox21, Sox15*
BMP signaling components, target genes and modulators	*Bmp2, Bmp4, Smoc2, Nog, Gata4, Gata5, Gata6, Msx1, Msx2, Hand1, Hand2, Hes1, Id3, Id4, Tgfb2, Tgfbr1, Tgfbr3, Vegfa, Vegfc, Dlx2, Dlx5, Smad6, Smad1, Smad9, Smad2, Smad7, Hey2, Twist1, Twist2, Acvr1, Mmp2, Postn, Flrt3, Bmp2k, Mef2a, Cited2*	*Bmp8a, Bmp8b, Id2, Cited1, Zic5*
Genes rich in amnion	*Tfap2a,Twist1,Flrt3*	
Pluripotency-associated markers		*Dppa2, Dppa4*
Collagens and integrins	*Col9a1, Col4a5, Col5a2, Col5a1, Col1a1, Col1a2, Col4a2, Col4a1, Col4a3bp, Col23a1, Col3a1, Col4a6, Col27a1, Col26a1, Col8a2, Itga8, Itgb1*	

Table S3. Differential expression analysis highlights (cut-off: padj. <0.05).

Table S4. Top 100 most differentially expressed gense in KO-SetA or KO-SetB versus Ctrl amnion samples (RNA-Seq).

Click here to Download Table S4

A

Gene ID	Gene Name	Ctrl 1.1	Ctrl 2.1	Ctrl 3.1	Ctrl 4.1	Ctrl 5.1	KO 1.2	KO 3.2	KO 6.2	KO 2.2	KO 4.2	KO 5.2
ENSMUSG00000029337	*Fgf5*	0.0463522	0.0463522	0.2781130	0.9270433	0.0463522	5.0987380	16.2232571	9.2240805	0.0463522	0.0463522	0.0463522
ENSMUSG00000037171	*Nodal*	0.2766748	0.0553350	0.0553350	0.0553350	0.0553350	3.6521080	2.9327534	3.6521080	0.0553350	1.2727043	0.0553350
ENSMUSG00000062327	*T*	36.756044	41.212840	20.981992	104.309046	12.519089	216.480080	1006.735027	279.426057	34.051921	38.909327	26.540468
ENSMUSG00000066652	*Lefty2*	0.9767862	0.0443994	0.0443994	2.3531667	0.7547893	24.3308558	12.3430254	2.3087673	1.2431824	0.4883931	0.0443994
ENSMUSG00000027186	*Elf5*	0.0591765	0.2564315	0.1972550	0.1972550	0.3156080	0.5128630	0.1183530	0.0591765	70.8145430	42.6465298	76.6335654
ENSMUSG00000021255	*Esrrb*	0.0958548	0.1533676	0.1533676	0.0191710	0.6134705	0.3450772	0.0958548	0.0191710	39.3963110	33.9709309	39.3963110
ENSMUSG00000047501	*Cldn4*	0.3191816	0.5106906	0.0638363	0.5745269	1.0213811	0.0638363	0.8937085	0.0638363	33.0033783	24.7684928	43.2810261
ENSMUSG00000074637	*Sox2*	3.6068608	6.5374352	4.0577184	6.8755784	1.5780016	3.2687176	18.9923764	3.8322896	92.9893799	35.2232500	56.0190567
				Ctrl				**KO-SetA**			**KO-SetB**	

B

Selected genes enriched in KO-SetA

Gene ID	Comparison	log$_2$ Fold Change	p.adj.
Fgf5	KO-setA vs Ctrl	6.16075779794208	1.81873385913884e-10
	KO-setB vs Ctrl	-1.74310062924334	0.331548627984435
	KO-SetB vs KO-SetA	-7.90385842718541	1.23115117082365e-08
Nodal	KO-setA vs Ctrl	4.59725897942216	0.000585195595286753
	KO-setB vs Ctrl	2.17085268679028	0.16287679917155
	KO-SetB vs KO-SetA	-2.42640629263189	0.150176193285943
T	KO-setA vs Ctrl	3.58132861465481	9.12924374983415e-07
	KO-setB vs Ctrl	-0.380749064181876	0.724006771706442
	KO-SetB vs KO-SetA	-3.96207767883669	1.00111017881162e-06
Lefty2	KO-setA vs Ctrl	4.51797067858599	0.000470896168512567
	KO-setB vs Ctrl	-0.418754191923372	0.834151087607506
	KO-SetB vs KO-SetA	-4.93672487050937	0.000734872133795889

Selected genes enriched in KO-SetB

Gene ID	Comparison	log$_2$ Fold Change	p.adj.
Elf5	KO-setA vs Ctrl	0.279899263412563	0.880161463820885
	KO-setB vs Ctrl	8.61394649337021	1.46436300266915e-34
	KO-SetB vs KO-SetA	8.33404722995764	8.15847149665294e-25
Esrrb	KO-setA vs Ctrl	-0.0178525607789109	0.992880455772707
	KO-setB vs Ctrl	7.65968085084086	3.64140098797345e-21
	KO-SetB vs KO-SetA	7.67753341161977	6.68665855440136e-16
Cldn4	KO-setA vs Ctrl	-0.446928095611415	0.819841766795906
	KO-setB vs Ctrl	6.0755960548316	2.80619696632073e-16
	KO-SetB vs KO-SetA	6.52252415044302	1.81992898403329e-12
Sox2	KO-setA vs Ctrl	1.03108493636301	0.359532368834508
	KO-setB vs Ctrl	3.92605097755526	5.49265480860401e-08
	KO-SetB vs KO-SetA	2.89496604119225	0.00136752480201529

Table S5. Comparative analysis of selected markers representative for KO-SetA and KO-SetB *Smad5* mutant amnion. (A) Normalized expression counts (FPKM) of individual RNA-Seq samples. (B) Comparison of differential expression of the selected markers between the three groups of replicates.

Clone	Embryo identity[1]	Mouse strain	Label	h, w (µm)[2]
1	039201	B6CBA[3]	LRDX	107,153
2	149103	B6CBA	LRDX	122,138
3	169204	B6CBA	LRDX	153,168
4	169205	B6CBA	LRDX	138,153
5	149211	B6CBA	LRDX	145,145
6	149201	B6CBA	LRDX	120,130
7	379107	B6CBA	LRDX	130,138
8	149217	B6CBA	LRDX	130,122
9	279216	B6CBA	LRDX	168,168
10	279211	B6CBA	LRDX	207,199
11	269205	B6CBA	LRDX	184,168
12	279215	B6CBA	LRDX	207,184
13	240104	B6CBA	HRP/LRDX	283,245
14	439005	B6CBA	LRDX	230,214
15	468506	Dub:ICR[4]	HRP/LRDX	na
16	518607	Dub:ICR	HRP/LRDX	209,221
17	359901	B6CBA	HRP/LRDX	260,230
18	528507	Dub:ICR	HRP/LRDX	na
19	128709	Dub:ICR	HRP/LRDX	353,379
20	269208	B6CBA	LRDX	184,199
21	269202	B6CBA	LRDX	230,199
22	409008	B6CBA	LRDX	122,153
23	280805	B6CBA	HRP/LRDX	214,191
24	190812	B6CBA	HRP/LRDX	184,230
25	410101	B6CBA	HRP/LRDX	367,283
26	828608	Dub:ICR	HRP/LRDX	412,279
27	190803	B6CBA	HRP/LRDX	237,199
28	269210	B6CBA	LRDX	230,161

Table S6. List of clones.

[1]The number is a unique embryo/clone identifier. [2]Height (h) and width (w) of the embryonic portion at dissection. [3]C57BL/6 x CBA.Ca or F1 matings. [4]Dub:ICR embryos are larger than BL6CBA, but less developmentally advanced, during E6 - E7.5.

Gene	Forward primer 5' – 3'	Reverse primer 5' – 3'
RT-qPCR		
Postn	AAGGAAAAGGGTCATACACGTACTTC	CCTCTGCGAATGTCAGAATCC
Tbx4	TCAACACCTTCCCAACTCAG	GGGAGAACGGAAATAGTGATCG
ζ-globin	GCTTCAAGATCATGACCGCCGT	CGGTGGAGGCTTAGCGGTACTT
Esrrb	CCATGCACAAACTCTTCCTG	CACTTGGATCGTGTCCGTC
Gapdh	AAGAAGGTGGTGAAGCAGGC	GCCTCTCTTGCTCAGTGTCC
Psmd4	GTTCCTTCAGAGCGTCCTAG	CTATCCAACCCCGTCTTTACAG
Nodal	AAAAGTGTTGGCATCAGCCC	TGGTGCTGGCGACAGGTAC
Lefty2	TCCTTGCCCATGATTGTCAG	CTGACGAGAGCACTAAGTTAGG
T	AACAGCTCTCCAACCTATGC	TACCATTGCTCACAGACCAG
Elf5	CCGAGTGGTTAAGTCAGAAGC	CGGTGTCCATCAGAGTTTCTC
Cldn4	CCGCCAGCAACTATGTGTAAG	ACGGGCTAGTAACTTTGCAC
Sox2	GATCAGCATGTACCTCCCC	CCCTCCCAATTCCCTTGTATC
Fgf5	ACTTTCCTTCACCGTCACTG	GTATCCGAGTTTCCTTCAGGG
Sex genotyping		
Jarid1cd	CTGAAGCTTTTGGCTTTGAG	CCACTGCCAAATTCTTTGG
Sry	TGGGACTGGTGACAATTGTC	GAGTACAGGTGTGCAGCTCT
IL3	GGGACTCCAAGCTTCAATCA	TGGAGGAGGAAGAAAGCAA
In situ hybridization		
Fgf5	ATTAACCCTCACTAAAGGGAAAACTC CATGCAAGTGCCAAA	TAATACGACTCACTATAGGGTTCC ACACGTGTAGGCACAG

Table S7. Lists of primers for RT-qPCR and sex genotyping PCR.

Supplementary Materials and Methods

Gene Set Enrichment Analyzis (GSEA).

To detect enriched functional gene sets, we ran GSEA (Subramanian et al., 2005) in PreRanked mode using the list of differentially expressed genes for each contrast (KO-SetA/Ctrl and KO-SetB/Ctrl) with padj. <0.05, ranked by the signed log of the adjusted p-value. The resulting ranked lists consisted of the genes with the "strongest" up-regulation in KO at the top of the list and the genes with the "strongest" down-regulation in KO at the bottom of the list, with the genes not changing among conditions in the middle. GSEA v.3.0 in PreRanked mode was run with the most recent version of Molecular Signatures Database (MSigDB)(Liberzon et al., 2011) – v.6.1 updated in October 2017, using the following collections of gene sets: Hallmark gene sets (Liberzon et al., 2016)(50 sets), C2 – Curated gene sets (4738 sets including Canonical pathways databases from BioCarta, KEGG and Reactome, and from expression signatures of genetic and chemical perturbations from biomedical literature), and C5 – 5917 Gene Ontology (GO) terms including all ontologies (molecular function, cellular component, and biological process)(Consortium, 2000). Gene size limits we set at 5 to 500. In addition, 4 custom made gene sets were used. Enrichment of each set of related genes in the top or bottom of the KO/ctrl ranked lists of genes was assessed by GSEA's normalized enrichment score (NES). The enrichment score reflects the degree to which a gene set is overrepresented at the top or bottom of a ranked list of genes. GSEA calculates the ES by walking down the ranked list of genes, increasing a running-sum statistic when a gene is in the gene set and decreasing it when it is not. The magnitude of the increment depends on the correlation of the gene with the phenotype. The ES is the maximum deviation from zero encountered in walking the list. A positive ES indicates gene set enrichment at the top of the ranked list; a negative ES indicates gene set enrichment at the bottom of the ranked list (Subramanian et al., 2005). The nominal p-value was used to estimate the statistical significance of the NES for each particular set.

References:

Consortium, T. G. O. (2000). Gene ontologie: Tool for the unification of biology. Nature Genetics **25**, 25–29.

Eakin, G. S., Hadjantonakis, A.-K., Papaioannou, V. E. and Behringer, **R. R.** (2005). Developmental potential and behavior of tetraploid cells in the mouse embryo. Developmental biology **288**, 150–9.

Gardner, R. L. and Cockroft, D. L. (1998). Complete dissipation of coherent clonal growth occurs before gastrulation in mouse epiblast. Development (Cambridge, England) **125**, 2397–2402.

Lawson, K. A. and Hage, W. J. (1994). Clonal analysis of the origin of primordial germ cells in the mouse. Ciba Foundation symposium **182**, 68-84-91.

Lawson, K. A., Meneses, J. J. and Pedersen, R. A. (1991). Clonal analysis of epiblast fate during germ layer formation in the mouse embryo. Development (Cambridge, England) **113**, 891–911.

McLaren, A. and Lawson, K.A. (2005). How is the mouse germ-cell lineage established? Differentiation **73,**435-7.

Liberzon, A., Subramanian, A., Pinchback, R., Thorvaldsdóttir, H., Tamayo, P. and Mesirov, J. P. (2011). Molecular signatures database (MSigDB) 3.0. Bioinformatics **27**, 1739–1740.

Liberzon, A., Birger, C., Ghandi, M., Jill, P., Tamayo, P., Jolla, L. and Jolla, L. (2016). Collection. **1**, 417–425.

Subramanian, A., Tamayo, P., Mootha, V. K., Mukherjee, S., Ebert, B. L., Gillette, M. A., Paulovich, A., Pomeroy, S. L., Golub, T. R., Lander, E. S., et al. (2005). Gene set enrichment analysis: a knowledge-based approach for interpreting genome-wide expression profiles. Proceedings of the National Academy of Sciences of the United States of America **102**, 15545–50.

Tzouanacou, E., Wegener, A., Wymeersch, F. J., Wilson, V. and Nicolas, J. F. (2009). Redefining the Progression of Lineage Segregations during Mammalian Embryogenesis by Clonal Analysis. Developmental Cell **17**, 365–376.

Wen, D., Saiz, N., Rosenwaks, Z., Hadjantonakis, A. K. and Rafii, S. (2014). Completely ES cell-derived mice produced by tetraploid complementation using inner cell mass (ICM) deficient blastocysts. PLoS ONE **9,** e94730.